

# Universal MIMO Jammer Mitigation

Gian Marti and Christoph Studer

**Abstract**—Multi-antenna processing enables jammer mitigation through spatial filtering, provided that the receiver knows the spatial signature of the jammer interference. Estimating this signature is easy for barrage jammers that transmit continuously and with static signature, but difficult for more sophisticated jammers. Smart jammers may deliberately suspend transmission when the receiver tries to estimate their spatial signature, or they may use time-varying beamforming to continuously change their spatial signature. To deal with such smart jammers, we propose MASH, the first method that indiscriminately mitigates *all* types of jammers. Assume that the transmitter and receiver share a common secret. Based on this secret, the transmitter *embeds* (with a time-domain transform) its signal in a secret subspace of a higher-dimensional space. The receiver applies a reciprocal transform to the receive signal, which (i) *raises* the legitimate transmit signal from its secret subspace and (ii) provably transforms *any* jammer into a barrage jammer, making estimation and mitigation via multi-antenna processing straightforward. Focusing on the massive multi-user MIMO uplink, we present three MASH-based data detectors and show their jammer-resilience via extensive simulations. We also introduce strategies for multi-user communication without a global secret as well as methods that use computationally efficient embedding and raising transforms.

**Index Terms**—Universal MIMO jammer mitigation

## I. INTRODUCTION

**D**ESPITE focusing on ultra-reliable communications as one of its main use-cases [2], 5G remains critically vulnerable against jamming attacks [3]–[5]. It is therefore imperative that next-generation wireless networks are able to mitigate jammers. Techniques such as direct-sequence spread spectrum (DSSS) [6], [7] or frequency-hopping spread spectrum (FHSS) [8], [9] provide a certain degree of robustness against interference, but are no match for strong wideband jammers. Multi-antenna (MIMO) processing, in contrast, is able to completely remove jammer interference through spatial filtering [10] and is therefore a promising path towards jammer-resilient communications. However, MIMO jammer mitigation relies on accurate knowledge of the jammer’s spatial signature (e.g., its subspace or its spatial covariance matrix) at the receiver. This signature is easy to estimate for barrage jammers (i.e., jammers that transmit continuously and with time-invariant signature): The receiver can analyze the receive signal from a dedicated training period, which provides a representative snapshot of the jammer’s spatial signature. A more sophisticated jammer, however, may thwart such a naïve approach, for example by deliberately suspending jamming during the training period, by manipulating its spatial signature through time-varying beamforming, or by jamming only specific communication

parts (e.g., control signals) and staying unnoticeable during other parts [3], [11], [12]. In all such cases, the signal received during training does *not* provide a representative snapshot of the jammer’s spatial signature.

## A. Contributions

We propose MASH (short for MitigAtion via Subspace Hiding), the first approach for MIMO jammer mitigation that mitigates *all* types of jammers, no matter how “smart” they are. MASH assumes that the transmitter(s) and the receiver share a common secret. Based on this secret, the transmitter(s) *embed* their time-domain signals in a secret subspace of a higher-dimensional space using a linear time-domain transform; the receiver then applies an inverse linear time-domain transform to the receive signal. We show that the receiver’s transform (i) *raises* the legitimate transmit signal from its secret subspace and (ii) provably transforms *any* jammer into a barrage jammer, which enables simplified mitigation. To showcase the effectiveness of MASH, we consider data transmission in the massive multi-user MIMO uplink. We provide three MASH-based data detectors for this scenario, and we show their resilience against a range of jammers in extensive simulations.

In addition to the material contained in the conference version [1], this paper makes the following additional contributions: We present a new result (Proposition 1) which proves that single-antenna barrage jammers can easily and effectively be mitigated. This result underpins our claim that, by transforming them into barrage jammers, MASH makes *all* jammers easy to mitigate. We also propose reciprocal MASH, a strategy for using MASH in the practically relevant multi-user scenario in which the receiver shares a common secret with every transmitter, but where these secrets are pairwise distinct. Finally, we introduce computationally efficient transforms (which approximate the theoretically optimal ones) for embedding and raising.

## B. State of the Art

The potential of MIMO processing for jammer mitigation is well known [13]. A variety of methods have been proposed that aim at mitigating barrage jammers [14]–[24], which either assume perfect knowledge of the jammer’s spatial signature at the receiver [14]–[17] or exploit the jammer’s stationarity by using a training period [18]–[24]. References [18]–[20] estimate the jammer’s spatial signature during a dedicated training period in which the legitimate transmitters are idle. References [21], [22] estimate the jammer’s spatial signature during a prolonged pilot phase in which the jammer interference is separated from the legitimate transmit signals by projecting the receive signals onto an unused pilot sequence that is orthogonal to the legitimate pilots. References [23], [24] propose a jammer-resilient data detector directly as a function of

The authors are with the Department of Information Technology and Electrical Engineering, ETH Zurich. (email: marti@iis.ee.ethz.ch, studer@ethz.ch)  
The work of GM and CS was supported in part by an ETH Research Grant. A short version of this paper was presented at the 57th Asilomar Conference on Signals, Systems, and Computers [1].

Emojis by Twitter, Inc. and other contributors are licensed under CC-BY 4.0.

certain spatial filters which are estimated during the pilot phase. While all of these methods are only effective against barrage jammers, MASH transforms *any* jammer into a barrage jammer and therefore can be used to make the aforementioned methods effective also for the mitigation of non-barrage jammers.

It is widely known that jammers do not need to transmit in a time-invariant manner. Several MIMO methods have been proposed for mitigating time-varying jammers [25]–[30]. References [25], [26] consider a jammer that only jams when the legitimate transmitters are active. Corresponding mitigation methods use a training period in which the legitimate transmitters send pre-defined symbols that can be compensated for at the receiver. References [27], [28] assume a multi-antenna jammer that continuously alters its spatial interference subspace through time-varying beamforming. Corresponding mitigation methods use a training period (in which the legitimate transmitters are idle) recurrently and whenever the jammer subspace is believed to have changed substantially. References [29], [30] consider general smart jammers. To mitigate such jammers, they propose a novel paradigm called joint jammer mitigation and data detection (JMD) in which the jammer subspace is estimated and nulled jointly with detecting the transmit data over an entire communication frame. MASH is complementary to JMD, and the two can be productively combined (cf. Section IV-C).

All of the above methods make stringent assumptions about the jammer’s transmit behavior (i.e., that the jammer is a barrage [14], [16]–[24] or reactive jammer [25], [26], or that the jammer’s beamforming changes only slowly over time [27], [28]), or they require solving a complex optimization problem while still being susceptible to certain types of jammers [29], [30]. Moreover, the number of jammer antennas is often required to be known in advance (see e.g., [22], [26], [30]). MASH, in contrast, makes *no* assumptions about the jammer’s transmit behavior, does *not* require solving an optimization problem, is effective against *all* jammer types, and does *not* require the number of jammer antennas to be known a priori.<sup>1</sup>

### C. Notation

Matrices and column vectors are represented by boldface uppercase and lowercase letters, respectively. For a matrix  $\mathbf{A}$ , the transpose is  $\mathbf{A}^T$ , the conjugate transpose is  $\mathbf{A}^H$ , the pseudoinverse is  $\mathbf{A}^\dagger$ , the submatrix consisting of the columns (or rows) from  $n$  through  $m$  is  $\mathbf{A}_{[n:m]}$  (or  $\mathbf{A}_{(n:m)}$ , respectively), the spectral norm is  $\|\mathbf{A}\|$ , and the Frobenius norm is  $\|\mathbf{A}\|_F$ . For a vector  $\mathbf{a}$ , the Euclidean norm is  $\|\mathbf{a}\|_2$ . The columnspace and row space of  $\mathbf{A}$  are  $\text{col}(\mathbf{A})$  and  $\text{row}(\mathbf{A})$ , respectively. Horizontal concatenation of two matrices  $\mathbf{A}$  and  $\mathbf{B}$  is denoted by  $[\mathbf{A}, \mathbf{B}]$ ; vertical concatenation is  $[\mathbf{A}; \mathbf{B}]$ . The  $k$ th column and row of  $\mathbf{A}$  are  $\mathbf{a}_k$  and  $\mathbf{a}_{(k)}^T$ , respectively. The  $N \times N$  identity matrix is  $\mathbf{I}_N$ ; the  $M \times N$  all-zero matrix is  $\mathbf{0}_{M \times N}$ . The compact singular value decomposition (SVD) of a rank- $R$  matrix  $\mathbf{A} \in \mathbb{C}^{M \times N}$  is denoted  $\mathbf{A} = \mathbf{U}\mathbf{\Sigma}\mathbf{V}^H$ , where  $\mathbf{U} \in \mathbb{C}^{M \times R}$  and  $\mathbf{V} \in \mathbb{C}^{N \times R}$  have orthonormal columns and  $\mathbf{\Sigma} \in \mathbb{R}^{R \times R}$  is a diagonal matrix whose diagonal entries are the positive singular values of

<sup>1</sup>It is important to not confound MASH with DSSS: DSSS transforms transmit symbols *individually*, while MASH transforms entire blocks of symbols. Crucially, this means that DSSS does *not* transform smart jammers into barrage jammers—this in stark contrast to MASH.

$\mathbf{A}$  in decreasing order. The main diagonal of  $\mathbf{\Sigma}$  is denoted by  $\boldsymbol{\sigma} = \text{diag}(\mathbf{\Sigma})$ . The distribution of a circularly-symmetric complex Gaussian random vector with covariance matrix  $\mathbf{C}$  is  $\mathcal{CN}(\mathbf{0}, \mathbf{C})$ .  $[1 : N]$  are the integers from 1 through  $N$ .

## II. SYSTEM MODEL

We consider jammer mitigation in communication systems with a multi-antenna receiver. Due to its relevance for next generation wireless networks, we focus on the multi-user (MU) MIMO uplink. But we emphasize that our method can also be applied in single-user (SIMO) or point-to-point MIMO settings. We consider a frequency-flat transmission model<sup>2</sup> with the following input-output relation:

$$\mathbf{y}_k = \mathbf{H}\mathbf{x}_k + \mathbf{J}\mathbf{w}_k + \mathbf{n}_k. \quad (1)$$

Here,  $\mathbf{y}_k \in \mathbb{C}^B$  is the time- $k$  receive vector at the basestation (BS);  $\mathbf{H} \in \mathbb{C}^{B \times U}$  is the channel matrix of  $U$  legitimate single-antenna user equipments (UEs) with time- $k$  transmit vector  $\mathbf{x}_k \in \mathbb{C}^U$ ;  $\mathbf{J} \in \mathbb{C}^{B \times I}$  is the channel matrix of an  $I$ -antenna jammer (or of multiple jammers, with  $I$  being the total number of jammer antennas) with time- $k$  transmit vector  $\mathbf{w}_k \in \mathbb{C}^I$ ; and  $\mathbf{n}_k \sim \mathcal{CN}(\mathbf{0}, N_0\mathbf{I}_B)$  is i.i.d. circularly-symmetric complex white Gaussian noise with per-entry variance  $N_0$ . The channel matrices  $\mathbf{H}$  and  $\mathbf{J}$  are assumed to stay constant for a coherence interval consisting of multiple channel uses. We assume that the jammer can vary its transmit characteristics. For this, we use a model in which the jammer transmits

$$\mathbf{w}_k = \mathbf{A}_k \tilde{\mathbf{w}}_k \quad (2)$$

at time  $k$ , where, without loss of generality,  $\mathbb{E}[\tilde{\mathbf{w}}_k \tilde{\mathbf{w}}_k^H] = \mathbf{I}_I$  for all  $k$ , and where  $\mathbf{A}_k \in \mathbb{C}^{I \times I}$  is a beamforming matrix that can change *arbitrarily* as a function of  $k$ . In particular,  $\mathbf{A}_k$  can be the all-zero matrix (the jammer suspends jamming at time  $k$ ), some of its rows can be zero (the jammer uses only a subset of its antennas at time  $k$ ), or it can be rank-deficient in another way. There need not be any relation between  $\mathbf{A}_k$  and  $\mathbf{A}_{k'}$  for  $k \neq k'$ . Our only restriction is that the number of jammer antennas  $I$  is smaller than the number of BS antennas  $B$ .

Unless noted otherwise, we assume that the UEs and the BS are jointly synchronized. Our proposed method operates on transmission frames of length  $L$ , where  $L$  does not exceed the length  $L_c$  of a coherence interval. Therefore, the channel matrices  $\mathbf{H}$  and  $\mathbf{J}$  are constant for the duration of a frame, and we restate (1) for a length- $L$  transmission frame as

$$\mathbf{Y} = \mathbf{H}\mathbf{X} + \mathbf{J}\mathbf{W} + \mathbf{N}, \quad (3)$$

where  $\mathbf{Y} = [\mathbf{y}_1, \dots, \mathbf{y}_L] \in \mathbb{C}^{B \times L}$  is the receive matrix, and  $\mathbf{X} = [\mathbf{x}_1, \dots, \mathbf{x}_L] \in \mathbb{C}^{U \times L}$  and  $\mathbf{W} = [\mathbf{A}_1 \tilde{\mathbf{w}}_1, \dots, \mathbf{A}_L \tilde{\mathbf{w}}_L] \in \mathbb{C}^{I \times L}$  are the corresponding transmit matrices. Since we do not impose any restriction on the matrices  $\mathbf{A}_k$ ,  $\mathbf{W}$  can be arbitrary and need in general not follow an explicit probabilistic model.

## III. ON BARRAGE JAMMERS

We prepare the ground for the exposition of MASH by considering a class of jammers that is easy to mitigate: *barrage jammers*. Such jammers transmit noise-like stationary signals

<sup>2</sup>An extension to frequency-selective channels with OFDM is possible [31].

over the entire spectrum [12], which appear as white (with respect to time) noise in the baseband representation (3). Per se, the notion of barrage jammers neither includes nor excludes the use of transmit beamforming.

We now introduce a formal notion of barrage jammers. This notion explicitly allows for transmit beamforming, as long as the beams stay constant for the duration of a communication frame. Following our model in Section II, we consider communication in frames of length  $L$ . During such a frame, a jammer transmits some matrix  $\mathbf{W} \in \mathbb{C}^{I \times L}$  with corresponding receive interference  $\mathbf{JW} \in \mathbb{C}^{B \times L}$ . We denote by  $I^*$  the rank of  $\mathbf{JW}$ , i.e.,  $I^*$  is the dimension of the interference space which, depending on the jammer's transmit beamforming type, can be equal to or strictly smaller than  $I$ . We now consider the compact SVD of the interference, which we write as

$$\mathbf{JW} = \mathbf{U}\mathbf{\Sigma}\mathbf{V}^H. \quad (4)$$

We call  $\mathbf{U} \in \mathbb{C}^{B \times I^*}$  the *spatial scope* of the jammer: The columns of this matrix form an orthonormal basis of the interference space in the spatial domain. We call  $\mathbf{V} \in \mathbb{C}^{L \times I^*}$  the *temporal extension* of the jammer within the frame: its columns form an orthonormal basis of the interference space in the time domain. Finally, we call  $\boldsymbol{\sigma} = \text{diag}(\mathbf{\Sigma}) = [\sigma_1, \dots, \sigma_{I^*}]^T$  (with  $\sigma_1 \geq \dots \geq \sigma_{I^*} > 0$ ) the *energy profile*, which determines how much energy the jammer allocates to the different dimensions in space and time. While the decomposition of the receive interference in (4) does not necessarily assume a probabilistic jamming model, our definition of barrage jammers is more narrow and explicitly requires a certain probabilistic behavior:

**Definition 1** (Barrage jammer). *A barrage jammer is a jammer for which the columns of  $\mathbf{V}$  are distributed uniformly over the complex  $L$ -dimensional unit sphere.*

Barrage jammers are fully characterized by their spatial scope  $\mathbf{U}$  and their energy profile  $\boldsymbol{\sigma}$ . Examples are a jammer that transmits  $\mathbf{W}$  with i.i.d.  $\mathcal{CN}(0, 1)$  entries or a jammer that transmits  $\mathbf{W} = \mathbf{a}\mathbf{w}^T$ , with  $\mathbf{a} \in \mathbb{C}^I$  and with  $\mathbf{w} \sim \mathcal{CN}(\mathbf{0}, \mathbf{I}_B)$ .

Such a formal definition of barrage jammers allows us to see why barrage jammers can be mitigated easily and effectively: Consider a length- $L$  communication frame as in (3), where the jammer is a barrage jammer with compact SVD as given in (4). For simplicity, let us temporarily neglect the impact of thermal noise by assuming  $\mathbf{N} = \mathbf{0}$ . If we insert a jammer training period of duration  $R$  at the start of the frame, i.e., if the first  $R$  columns of  $\mathbf{X}$  in (3) are zero, then the corresponding receive signal is

$$\mathbf{Y}_{[1:R]} = \mathbf{JW}_{[1:R]} = \mathbf{U}\mathbf{\Sigma}(\mathbf{V}^H)_{[1:R]}. \quad (5)$$

Since the columns of  $\mathbf{V}$  are uniformly distributed over the complex  $L$ -dimensional unit sphere, the truncated temporal extension  $(\mathbf{V}^H)_{[1:R]} \in \mathbb{C}^{I^* \times R}$  has full rank  $\min\{I^*, R\}$  with probability one. So provided that  $I^* \leq R$ , we have  $\text{col}(\mathbf{Y}_{[1:R]}) = \text{col}(\mathbf{U})$  with probability one. Thus, the receiver can find the jammer subspace  $\text{col}(\mathbf{JW})$  of the entire frame from the compact SVD  $\mathbf{Y}_{[1:R]} = \tilde{\mathbf{U}}\tilde{\mathbf{\Sigma}}\tilde{\mathbf{V}}^H$  as  $\text{col}(\mathbf{JW}) = \text{col}(\tilde{\mathbf{U}})$ , and it can mitigate the jammer for the entire frame using a projection matrix  $\mathbf{P} = \mathbf{I}_B - \tilde{\mathbf{U}}\tilde{\mathbf{U}}^H$ , which satisfies  $\mathbf{P}\mathbf{JW} = \mathbf{0}_{B \times L}$ .

A smart or dynamic jammer, in contrast, might stop jamming

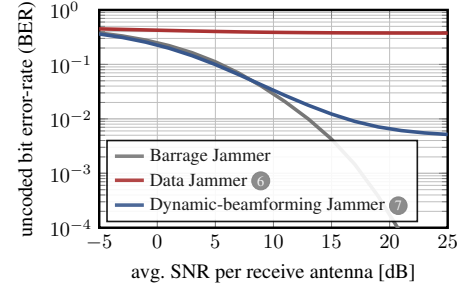


Fig. 1. Error-rate performance of a coherent communication receiver that uses a training-period-based orthogonal projection for mitigating the jammer, least squares channel estimation, and LMMSE data detection. The setup is described in Section VI and the 10-antenna jammers are a barrage jammer transmitting i.i.d.  $\mathcal{CN}(0, 1)$  symbols as well as the jammers 6 and 7 from Section VI-C.

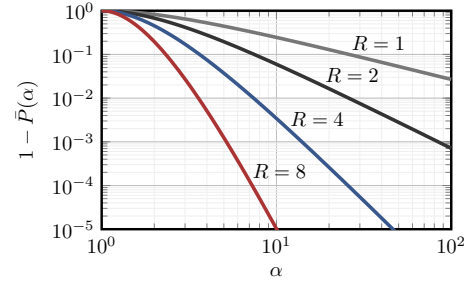


Fig. 2. Probability bound  $1 - \bar{P}(\alpha)$  that the residual interference power bound in (6) does not hold, as a function of the threshold  $\alpha$ , and for different redundancies  $R$ . As in Section VI, the frame length is  $L = 100$ . Note that the curves' asymptotic slope of descent (in doubly-logarithmic scale) coincides with  $R$ , so that the redundancy  $R$  plays a role that is analogous to diversity.

during these  $R$  training samples, in which case (5) amounts to  $\mathbf{Y}_{[1:R]} = \mathbf{0}_{B \times R}$  so that the projection  $\mathbf{P} = \mathbf{I}_B$  is simply the identity, which will not mitigate any subsequent interference of the jammer, since  $\mathbf{P}\mathbf{JW}_{[R+1:L]} = \mathbf{JW}_{[R+1:L]}$ .

Similarly, a dynamic multi-antenna jammer could at any given instant use only a subset of its antennas but switch between different subsets over time, thereby changing the spatial subspace of its interference. If  $\text{col}(\mathbf{W}_{[1:R]}) \not\subseteq \text{col}(\mathbf{W}_{[R+1:L]})$  and the columns of  $\mathbf{J}$  are linearly independent, then  $\text{col}(\mathbf{JW}_{[1:R]}) \not\subseteq \text{col}(\mathbf{JW}_{[R+1:L]})$ , so the projection  $\mathbf{P}$  will not completely mitigate the jammer,  $\mathbf{P}\mathbf{JW}_{[R+1:L]} \neq \mathbf{0}_{B \times (L-R)}$ .

Fig. 1 shows the effectiveness of jammer mitigation with an orthogonal projection based on a training period for a barrage jammer as well as for two non-barrage jammers (the simulations of Fig. 1 do take into account the effects of thermal noise  $\mathbf{N}$ ).

For single-antenna jammers, we can also provide a theoretical guarantee for the mitigation of barrage jammers in the presence of noise. Specifically, we have the following guarantee:<sup>3</sup>

**Proposition 1.** *Consider a single-antenna barrage jammer with channel vector  $\mathbf{j} \in \mathbb{C}^B$  and frame transmit signal  $\mathbf{w}^T \in \mathbb{C}^L$ , so that the interference is  $\mathbf{j}\mathbf{w}^T$ . Let  $\mathbf{N} \in \mathbb{C}^{B \times L}$  be the receive noise. Assume that (i) the first  $R$  samples of the frame are used as a jammer training period during which the UEs are silent, (ii) the receiver estimates the jammer subspace as the leading left-singular vector  $\mathbf{u}_1$  of the training period receive signal  $(\mathbf{j}\mathbf{w}^T + \mathbf{N})_{[1:R]}$ , and (iii) the receiver mitigates the jammer*

<sup>3</sup>We conjecture that an analogous result holds also for multi-antenna barrage jammers, but that case presents substantial additional analytical difficulties.

in that frame with a projection  $\mathbf{P} = \mathbf{I}_B - \mathbf{u}_1 \mathbf{u}_1^H$ . Then, for any threshold  $\alpha > 1$ , the residual interference power after projecting satisfies

$$\frac{\|\mathbf{P}\mathbf{j}\mathbf{w}^T\|_F^2}{L} \leq 12\alpha \frac{\|\mathbf{N}_{[1:R]}\|_F^2}{R} \quad (6)$$

with probability at least  $\bar{P}(\alpha) = 1 - \alpha^{-R} \left(\frac{L-R/\alpha}{L-R}\right)^{L-R}$ .

(Note that the guarantees of Proposition 1 can be tightened at the expense of intuitiveness; the interested reader may consult the proof in Appendix A for the details.) For a single-antenna barrage jammer, the probability that the residual interference power  $\|\mathbf{P}\mathbf{j}\mathbf{w}^T\|_F^2/L$  after mitigation exceeds some value proportional to the training noise power  $\|\mathbf{N}_{[1:R]}\|_F^2/R$  decreases polynomially with order  $R$  (the length of the training period); cf. Fig. 2. Note that the bound for the residual jammer energy does not depend on the jammer transmit power, nor on the jammer's channel gain, since a larger jammer receive power yields a more accurate estimate of the jammer subspace, which leads to proportionally more effective mitigation.

#### IV. MASH: UNIVERSAL MIMO JAMMER MITIGATION VIA SECRET TEMPORAL SUBSPACE EMBEDDINGS

We are now ready to present MASH. We assume that the UEs and the BS share a common secret  $\clubsuit$ . Based on this secret, the UEs and the BS construct, in pseudo-random manner, a unitary matrix  $\mathbf{C} = f(\clubsuit)$ , which is uniformly (or *Haar*) distributed over the set of all unitary  $L \times L$  matrices.<sup>4</sup> Since the jammer does not know the common secret  $\clubsuit$ , it does not know  $\mathbf{C}$ . The matrix  $\mathbf{C}$  is then divided row-wise into two submatrices  $\mathbf{C} = [\mathbf{C}_\perp; \mathbf{C}_\parallel]$  with  $\mathbf{C}_\perp \in \mathbb{C}^{R \times L}$  and  $\mathbf{C}_\parallel \in \mathbb{C}^{(L-R) \times L}$ , where  $R$  and  $K$  are non-negative integers such that  $R + K = L$ . We call  $R$  the *redundancy*, and we require that  $R \geq I^*$ , i.e., that the redundancy is at least as big as the rank of the interference.<sup>5</sup>

The UEs use the matrix  $\mathbf{C}_\parallel$  to *embed* a length- $K$  message signal  $\mathbf{S} \in \mathbb{C}^{U \times K}$  in the secret  $K$ -dimensional subspace of  $\mathbb{C}^L$  that is spanned by the rows of  $\mathbf{C}_\parallel$  by transmitting

$$\mathbf{X} = \mathbf{S}\mathbf{C}_\parallel. \quad (7)$$

The message signal  $\mathbf{S}$  could consist, e.g., of pilots for channel estimation, control signals, or data symbols. Embedding  $\mathbf{S}$  into the secret subspace requires no cooperation between the UEs: The  $u$ th UE simply transmits the  $u$ th row of  $\mathbf{X}$ , which it can compute as  $\mathbf{x}_{(u)}^T = \mathbf{s}_{(u)}^T \mathbf{C}_\parallel$ , where  $\mathbf{s}_{(u)}^T$  is its own message signal. With  $\mathbf{X}$  as in (7), the receive matrix in (3) becomes

$$\begin{aligned} \mathbf{Y} &= \mathbf{H}\mathbf{X} + \mathbf{J}\mathbf{W} + \mathbf{N} \\ &= \mathbf{H}\mathbf{S}\mathbf{C}_\parallel + \mathbf{J}\mathbf{W} + \mathbf{N}. \end{aligned} \quad (8)$$

Since  $\mathbf{C}$  is unknown to the jammer,  $\mathbf{W}$  is independent of  $\mathbf{C}$ . (This does not imply a probabilistic model for  $\mathbf{W}$ —it only

<sup>4</sup>See [32, Sec. 1.2] on how to construct Haar distributed matrices.

<sup>5</sup>We do not require this dimension to be known a priori. The choice of  $R$  simply limits number of interference dimensions that can be mitigated. We note that the number of interference dimensions  $I^*$  that can be mitigated with spatial filtering is fundamentally (i.e., not just for MASH) limited by both the channel coherence time  $L_c$  as well as the number of receive antennas  $B$  (this is easy to show). The fact that MASH requires  $I^* \leq R \leq L_c$  is thus due to communication-theoretic limits, and not due to a drawback of MASH itself.

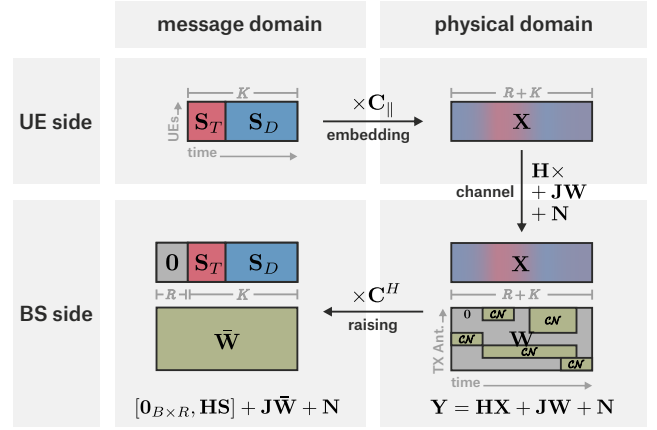


Fig. 3. Structural diagram of MASH. Here, the UE message signal  $\mathbf{S}$  consists of pilots  $\mathbf{S}_T$  (shown in red) and data symbols  $\mathbf{S}_D$  (shown in blue). The jammer is a multi-antenna jammer that dynamically switches different antennas off (shown in gray) while transmitting Gaussian symbols using its active antennas (shown in green). Raising transforms the jammer into a barrage jammer.

means that  $\mathbf{W}$  is no function of  $\mathbf{C}$ .) We make no other assumptions about  $\mathbf{W}$ . In particular, we also allow that  $\mathbf{W}$  might depend on  $\mathbf{H}$  and  $\mathbf{J}$  (the jammer has full channel knowledge), or even on  $\mathbf{S}$  (the jammer knows the message to be transmitted).

Having received  $\mathbf{Y}$  as in (9), the receiver *raises* the signals by multiplying  $\mathbf{Y}$  from the right with  $\mathbf{C}_\parallel^H$ , obtaining

$$\bar{\mathbf{Y}} \triangleq \mathbf{Y}\mathbf{C}_\parallel^H = \mathbf{H}\mathbf{S}\mathbf{C}_\parallel\mathbf{C}_\parallel^H + \mathbf{J}\underbrace{\mathbf{W}\mathbf{C}_\parallel^H}_{\triangleq \bar{\mathbf{W}}} + \underbrace{\mathbf{N}\mathbf{C}_\parallel^H}_{\triangleq \bar{\mathbf{N}}} \quad (10)$$

$$= [\mathbf{0}_{B \times R}, \mathbf{H}\mathbf{S}] + \mathbf{J}\bar{\mathbf{W}} + \bar{\mathbf{N}}, \quad (11)$$

where  $\mathbf{C}_\parallel\mathbf{C}_\parallel^H = [\mathbf{0}_{K \times R}, \mathbf{I}_K]$  in (11) follows from the unitarity of  $\mathbf{C} = [\mathbf{C}_\perp; \mathbf{C}_\parallel]$ . We obtain an input-output relation in which the channels  $\mathbf{H}$  and  $\mathbf{J}$  are unchanged, the UEs are idle during the first  $R$  samples and transmit  $\mathbf{S}$  in the remaining  $K$  samples, the jammer transmits  $\bar{\mathbf{W}} = \mathbf{W}\mathbf{C}_\parallel^H$ , and the noise  $\bar{\mathbf{N}} = \mathbf{N}\mathbf{C}_\parallel^H$  retains its statistics and is i.i.d. circularly-symmetric complex Gaussian with per-entry variance  $N_0$ . We call the domain of the input-output relation (11) the *message domain*, which contrasts with the *physical domain* of (9); cf. Fig. 3. We now state our key theoretical result; the proof is in Appendix B:

**Theorem 1.** Consider the decomposition of the physical domain jammer interference  $\mathbf{J}\mathbf{W}$  in (9) into its spatial scope  $\mathbf{U}$ , its temporal extension  $\mathbf{V}$ , and its energy profile  $\sigma$ . Then the jammer interference  $\mathbf{J}\bar{\mathbf{W}}$  in the message domain (11) has identical spatial scope  $\bar{\mathbf{U}} = \mathbf{U}$  and energy profile  $\bar{\sigma} = \sigma$ , but its temporal extension  $\bar{\mathbf{V}}$  is a random matrix whose columns are uniformly distributed over the complex  $L$ -dimensional unit sphere. Thus,  $\mathbf{J}\bar{\mathbf{W}}$  is barrage jammer interference according to Definition 1.

Put simply, MASH transforms any jammer into the (unique) barrage jammer with identical spatial scope and identical energy profile.<sup>6</sup> Furthermore, we see in the message-domain input-output relation (11) that MASH also conveniently deals with the legitimate transmit signals: The first  $R$  columns of the message domain receive signal  $\bar{\mathbf{Y}}$  contain no UE signals and thus correspond to a jammer training period which can be used

<sup>6</sup>The random behavior of barrage jammers (cf. Definition 1) is induced by the randomness of  $\mathbf{C}$  even if the jammer is deterministic in the physical domain.

for constructing a jammer-mitigating filter that is effective for the entire frame (since the message domain jammer is a barrage jammer). The remaining  $K$  columns of  $\bar{\mathbf{Y}}$  correspond to the transmit signal  $\mathbf{S}$ , which can be recovered using the jammer-mitigating filter from the training period.

To understand how MASH can be used for MIMO jammer mitigation, we consider the case of coherent data transmission, for which we propose three different ways to proceed from (11): (i) orthogonal projection, (ii) jammer-resilient LMMSE equalization, and (iii) joint jammer mitigation and data detection. In coherent data transmission, the transmit signal  $\mathbf{S} = [\mathbf{S}_T, \mathbf{S}_D]$  consists of orthogonal pilots  $\mathbf{S}_T \in \mathbb{C}^{U \times U}$  and data symbols  $\mathbf{S}_D \in \mathcal{S}^{U \times (K-U)}$  taken from a constellation  $\mathcal{S}$ . To simplify the ensuing discussion, we define  $[\bar{\mathbf{Y}}_J, \bar{\mathbf{Y}}_T, \bar{\mathbf{Y}}_D] \triangleq \bar{\mathbf{Y}}$  and rewrite (11) as three separate equations:

$$\bar{\mathbf{Y}}_J = \mathbf{J}\bar{\mathbf{W}}_J + \bar{\mathbf{N}}_J \in \mathbb{C}^{B \times R} \quad (12)$$

$$\bar{\mathbf{Y}}_T = \mathbf{H}\mathbf{S}_T + \mathbf{J}\bar{\mathbf{W}}_T + \bar{\mathbf{N}}_T \in \mathbb{C}^{B \times U} \quad (13)$$

$$\bar{\mathbf{Y}}_D = \mathbf{H}\mathbf{S}_D + \mathbf{J}\bar{\mathbf{W}}_D + \bar{\mathbf{N}}_D \in \mathbb{C}^{B \times (K-U)}. \quad (14)$$

### A. Orthogonal Projection

The matrix  $\bar{\mathbf{Y}}_J$  contains samples of a barrage jammer corrupted by white Gaussian noise  $\bar{\mathbf{N}}_J$ , but not by any UE signals. We can thus use  $\bar{\mathbf{Y}}_J$  to estimate the projection onto the orthogonal complement of the jammer's spatial scope (cf. Section III). The maximum-likelihood estimate of the jammer's spatial scope is given by the  $I^*$  leading left-singular vectors  $[\mathbf{u}_1, \dots, \mathbf{u}_{I^*}] \in \mathbb{C}^{B \times I^*}$  of  $\bar{\mathbf{Y}}_J$  [33]. The effective dimension  $I^*$  of the jammer interference is not known a priori. This quantity can, however, be estimated directly from  $\bar{\mathbf{Y}}_J$  as the number of singular values that significantly exceed the threshold  $\sqrt{BN_0}$  which is expected due to thermal noise:<sup>7</sup>

$$\hat{I}^* = \arg \max_i \sigma_i(\bar{\mathbf{Y}}_J) > \beta \sqrt{BN_0}, \quad (15)$$

where  $\sigma_i(\bar{\mathbf{Y}}_J)$  is the  $i$ th largest singular value of  $\bar{\mathbf{Y}}_J$ , and  $\beta$  is a tuneable threshold parameter (for instance,  $\beta = 2$  is a sensible choice). More complex methods, such as the Akaike information criterion (AIC) or the minimum description length (MDL) criterion, could also be used [34]. With this estimate  $\hat{I}^*$  of  $I^*$ , the estimate of jammer's spatial scope is given by the  $\hat{I}^*$  leading left-singular vectors  $\mathbf{U}(\bar{\mathbf{Y}}_J) \triangleq [\mathbf{u}_1, \dots, \mathbf{u}_{\hat{I}^*}] \in \mathbb{C}^{B \times \hat{I}^*}$  of  $\bar{\mathbf{Y}}_J$ . The corresponding projection matrix is therefore

$$\hat{\mathbf{P}} = \mathbf{I}_B - \mathbf{U}\mathbf{U}^H, \quad (16)$$

where the dependence of  $\mathbf{U} = \mathbf{U}(\bar{\mathbf{Y}}_J)$  on  $\bar{\mathbf{Y}}_J$  is left implicit, and the jammer can be mitigated in the pilot and data phases via

$$\bar{\mathbf{Y}}_{\mathbf{P},T} \triangleq \hat{\mathbf{P}}\bar{\mathbf{Y}}_T = \underbrace{\hat{\mathbf{P}}\mathbf{H}\mathbf{S}_T}_{\triangleq \mathbf{H}_{\mathbf{P}}} + \hat{\mathbf{P}}\mathbf{J}\bar{\mathbf{W}}_T + \underbrace{\hat{\mathbf{P}}\bar{\mathbf{N}}_T}_{\triangleq \mathbf{N}_{\mathbf{P},T}} \quad (17)$$

$$\approx \mathbf{H}_{\mathbf{P}}\mathbf{S}_T + \mathbf{N}_{\mathbf{P},T}, \quad (18)$$

and

$$\bar{\mathbf{Y}}_{\mathbf{P},D} \triangleq \hat{\mathbf{P}}\bar{\mathbf{Y}}_D = \hat{\mathbf{P}}\mathbf{H}\mathbf{S}_D + \hat{\mathbf{P}}\mathbf{J}\bar{\mathbf{W}}_D + \hat{\mathbf{P}}\bar{\mathbf{N}}_D \quad (19)$$

$$\approx \mathbf{H}_{\mathbf{P}}\mathbf{S}_D + \mathbf{N}_{\mathbf{P},D}. \quad (20)$$

<sup>7</sup>We have  $\mathbb{E}[\|\mathbf{N}\|_F^2] = BLN_0$ , and  $\mathbb{E}[\|\mathbf{N}\|_F^2]$  equals the sum over  $L$  squared nonzero singular values of  $\mathbf{N}$  (assuming  $L \leq B$ ). By dividing through  $L$ , the expected average of squared nonzero singular values is  $BN_0$ .

The approximations in (18) and (20) hold because  $\hat{\mathbf{P}}\mathbf{J}\bar{\mathbf{W}}_T \approx \mathbf{0}$  and  $\hat{\mathbf{P}}\mathbf{J}\bar{\mathbf{W}}_D \approx \mathbf{0}$ . The BS thus obtains an input-output relation that is approximately jammer-free and consists of a virtual channel  $\mathbf{H}_{\mathbf{P}}$  corrupted by Gaussian noise with spatial distribution  $\mathcal{CN}(\mathbf{0}, N_0\mathbf{P})$ . The receiver can now estimate the virtual channel  $\mathbf{H}_{\mathbf{P}}$ , e.g., using least-squares (LS), as follows:

$$\hat{\mathbf{H}}_{\mathbf{P}} = \bar{\mathbf{Y}}_{\mathbf{P},T}\mathbf{S}_T^\dagger. \quad (21)$$

The data symbols  $\mathbf{S}_D$  can then be detected using, e.g., the well-known linear minimum mean square error (LMMSE) detector:

$$\hat{\mathbf{S}}_D = (\hat{\mathbf{H}}_{\mathbf{P}}^H \hat{\mathbf{H}}_{\mathbf{P}} + N_0\mathbf{I}_U)^{-1} \hat{\mathbf{H}}_{\mathbf{P}}^H \bar{\mathbf{Y}}_{\mathbf{P},D}. \quad (22)$$

### B. Jammer-Resilient LMMSE Equalization

The orthogonal projection method from the previous subsection is highly effective. However, it requires the computation of a singular value decomposition (of  $\bar{\mathbf{Y}}_J$ ) and the explicit estimation of the jammer interference dimension  $I^*$ . Both of these requirements can be avoided if, instead of an orthogonal projection, one directly uses an LMMSE-type equalizer based on an estimate of the jammer's spatial covariance matrix  $\mathbf{C}_J \triangleq \mathbb{E}[\mathbf{J}\bar{\mathbf{W}}(\mathbf{J}\bar{\mathbf{W}})^H]$ . Such an estimate can be obtained directly from  $\bar{\mathbf{Y}}_J$  in (12) as follows:

$$\hat{\mathbf{C}}_J = \frac{1}{R} \bar{\mathbf{Y}}_J \bar{\mathbf{Y}}_J^H. \quad (23)$$

An "LMMSE-type" jammer-mitigating estimate of  $\mathbf{H}$  based on (13) is then (the impact of the thermal noise  $\bar{\mathbf{N}}_T$  is neglected)

$$\hat{\mathbf{H}} = \left( \mathbf{I}_B + \frac{1}{U} \hat{\mathbf{C}}_J \right)^{-1} \bar{\mathbf{Y}}_T \mathbf{S}_T^\dagger, \quad (24)$$

where the identity in the inverse represents the covariance matrix of the despread pilot signal, and the LMMSE estimate of the data  $\mathbf{S}_D$  based on (14) is

$$\hat{\mathbf{S}}_D = \hat{\mathbf{H}}^H (\hat{\mathbf{H}}\hat{\mathbf{H}}^H + N_0\mathbf{I}_B + \hat{\mathbf{C}}_J)^{-1} \bar{\mathbf{Y}}_D. \quad (25)$$

This approach would avoid the calculation of an SVD, but would instead require us to invert two matrices of size  $B \times B$  (in (24) and in (25)). However, using identities from [35], we can rewrite (24) and (25) as

$$\hat{\mathbf{H}} = (\mathbf{I}_B - \bar{\mathbf{Y}}_J(UR\mathbf{I}_R + \bar{\mathbf{Y}}_J^H \bar{\mathbf{Y}}_J)^{-1} \bar{\mathbf{Y}}_J^H) \bar{\mathbf{Y}}_T \mathbf{S}_T^\dagger \quad (26)$$

and

$$\mathbf{A} = \left( N_0\mathbf{I}_{U+R} + \left[ \frac{\hat{\mathbf{H}}^H}{\sqrt{R}} \bar{\mathbf{Y}}_J^H \right] \left[ \hat{\mathbf{H}}, \frac{1}{\sqrt{R}} \bar{\mathbf{Y}}_J \right] \right)^{-1} \left[ \frac{\hat{\mathbf{H}}^H}{\sqrt{R}} \bar{\mathbf{Y}}_J^H \right] \quad (27)$$

$$\hat{\mathbf{S}}_D = \mathbf{A}_{(1:U)} \bar{\mathbf{Y}}_D. \quad (28)$$

So we only need to invert an  $R \times R$  matrix (in (26)) and a  $(U+R) \times (U+R)$  matrix (in (27)). In contrast, the orthogonal projection approach would require computation of an SVD for  $B \times L$  matrix and the inverting a  $U \times U$  matrix (in (22)).

### C. Joint Jammer Mitigation and Data Detection (JMD)

JMD is a recent paradigm for smart jammer mitigation. In JMD, the jammer subspace is estimated and nulled (through an orthogonal projection) *jointly* with detecting the transmit data over an entire transmission frame [29], [30]. JMD operates by approximately solving a nonconvex optimization problem.



In principle, this paradigm can provide excellent performance *even without* any jammer training period at all (corresponding to  $R = 0$ ). However, JMD suffers from several limitations: (i) it performs poorly against jammers with very short duty cycle, (ii) it needs to know the dimension  $I^*$  of the jammer interference, and (iii) it does not reliably converge to the correct solution if  $I^*$  is large. All of these shortcomings can either be completely avoided (in case of (i)) or substantially alleviated (in case of (ii) and (iii)) if JMD is combined with MASH: (i) MASH transforms jammers with short duty cycles into fully non-sparse barrage jammers, (ii) in combination with non-zero redundancy ( $R > 0$ ),  $\bar{\mathbf{Y}}_J$  can be used to estimate the dimension of the jammer interference, and (iii)  $\bar{\mathbf{Y}}_J$  can be used for optimal initialization to improve performance against high-dimensional jammers.

We now show how MASH can be combined with the specific JMD-type methods SANDMAN and MAED from [30], [36]. SANDMAN uses a fixed LS channel estimate and then performs joint jammer mitigation and data detection by approximately solving an optimization problem that depends on the (unknown) transmit data and the (unknown) jammer-nulling projector. In contrast, MAED unifies not only jammer mitigation and data detection, but also channel estimation, by approximately solving an optimization problem that depends on the transmit data, the jammer-nulling projector, *and* the UE channel matrix.

The optimization problem to solve when combining MASH with SANDMAN is

$$\min_{\substack{\tilde{\mathbf{P}} \in \mathcal{G}_{B-\hat{I}^*}(\mathbb{C}^B), \\ \tilde{\mathbf{S}}_D \in \mathcal{S}^{U \times D}}} \|\tilde{\mathbf{P}}(\bar{\mathbf{Y}}_D - \hat{\mathbf{H}}\tilde{\mathbf{S}}_D)\|_{\text{F}}^2. \quad (29)$$

Here,  $\mathcal{G}_{B-\hat{I}^*}(\mathbb{C}^B) = \{\mathbf{I}_B - \mathbf{Q}\mathbf{Q}^\dagger : \mathbf{Q} \in \mathbb{C}^{B \times \hat{I}^*}\}$  is the Grassmannian manifold, i.e., the set of orthogonal projections onto  $(B - \hat{I}^*)$ -dimensional subspaces of  $\mathbb{C}^B$ , where  $\hat{I}^*$  is estimated from  $\bar{\mathbf{Y}}_J$  as in (15); and  $\hat{\mathbf{H}} = \bar{\mathbf{Y}}_T \mathbf{S}_T^\dagger$  is an LS channel estimate. This optimization problem can then be approximately solved as in [36, Alg. 2]. However, to improve robustness and speed of convergence even when facing many-antenna jammers,  $\tilde{\mathbf{P}}$  and  $\tilde{\mathbf{S}}_D$  should be initialized as in (16) and (22), respectively (and not to the initial values specified in [36, Alg. 2]). We call the algorithm that results from this procedure MASH-S; see Algorithm 1. The step size  $\tau^{(t)}$  on line 11 of Algorithm 1 can be chosen in a predetermined fashion or adaptively (e.g., using the Barzilai-Borwein strategy [37]). The function  $\text{prox}_g$  on line 11 of Algorithm 1 is the so-called proximal operator [38] of a suitably defined indicator function  $g$  (cf. [30], [36]) which acts entrywise on its input matrix. For QAM constellations, this entry-wise mapping can be written as

$$\text{prox}_g(\tilde{s}; \tau) = \begin{cases} \text{clip}\left(\frac{\tilde{s}}{1-\tau\alpha}; a\right) & \alpha\tau < 1 \\ \arg\min_{\tilde{x} \in \mathcal{S}} |\tilde{s} - \tilde{x}|^2 & \text{else,} \end{cases} \quad (30)$$

where  $\text{clip}(z; a)$  clips the real and imaginary part of  $z \in \mathbb{C}$  to the interval  $[-a, a]$ , with  $a$  being the ‘‘height/width’’ of the constellation  $\mathcal{S}$  (e.g., for unit symbol energy QPSK,  $a = \sqrt{2}$ ). The parameter  $\alpha \geq 0$  in (30) is a tunable parameter that pushes the symbol estimates towards the corners of the constellation, see [30], [36]. In this paper, we choose  $\alpha = 2.5$ .

---

### Algorithm 1 MASH-S

---

```

1: function MASH-S( $\bar{\mathbf{Y}}_J, \bar{\mathbf{Y}}_T, \bar{\mathbf{Y}}_D, \mathbf{S}_T, \beta\sqrt{BN_0}, t_{\max}$ )
2:  $\hat{\mathbf{H}} = \bar{\mathbf{Y}}_T \mathbf{S}_T^\dagger$ 
3:  $\hat{I}^* = \arg \max_{\sigma_i(\bar{\mathbf{Y}}_J) > \beta\sqrt{BN_0}} i$ 
4:  $\tilde{\mathbf{P}}^{(0)} = \mathbf{I}_B - \mathbf{U}\mathbf{U}^\text{H}$  // cf. (16)
5:  $\tilde{\mathbf{S}}_D^{(0)} = (\hat{\mathbf{H}}^\text{H}\tilde{\mathbf{P}}^{(0)}\hat{\mathbf{H}} + N_0\mathbf{I}_U)^{-1}\hat{\mathbf{H}}^\text{H}\tilde{\mathbf{P}}^{(0)}\bar{\mathbf{Y}}_D$ 
6: for  $t = 1$  to  $t_{\max}$  do
7:  $\tilde{\mathbf{E}}^{(t)} = [\bar{\mathbf{Y}}_T, \bar{\mathbf{Y}}_D] - \hat{\mathbf{H}}[\mathbf{S}_T, \tilde{\mathbf{S}}_D^{(t-1)}]$ 
8:  $\tilde{\mathbf{J}}^{(t)} = \text{APPROXSVD}(\tilde{\mathbf{E}}^{(t)}, \hat{I}^*)$  // cf. [36, Alg. 1]
9:  $\tilde{\mathbf{P}}^{(t)} = \mathbf{I}_B - \tilde{\mathbf{J}}^{(t)}(\tilde{\mathbf{J}}^{(t)})^\dagger$ 
10:  $\nabla f(\tilde{\mathbf{S}}_D^{(t-1)}) = -2\hat{\mathbf{H}}^\text{H}\tilde{\mathbf{P}}^{(t)}(\bar{\mathbf{Y}}_D - \hat{\mathbf{H}}\tilde{\mathbf{S}}_D^{(t-1)})$ 
11:  $\tilde{\mathbf{S}}_D^{(t)} = \text{prox}_g(\tilde{\mathbf{S}}_D^{(t-1)} - \tau^{(t)}\nabla f(\tilde{\mathbf{S}}_D^{(t-1)}); \tau^{(t)})$ 
12: end for
13: output:  $\tilde{\mathbf{S}}_D^{(t_{\max})}$ 
14: end function

```

---



---

### Algorithm 2 MASH-M

---

```

1: function MASH-M( $\bar{\mathbf{Y}}_J, \bar{\mathbf{Y}}_T, \bar{\mathbf{Y}}_D, \mathbf{S}_T, \beta\sqrt{BN_0}, t_{\max}$ )
2:  $\hat{\mathbf{H}} = \bar{\mathbf{Y}}_T \mathbf{S}_T^\dagger$ 
3:  $\hat{I}^* = \arg \max_{\sigma_i(\bar{\mathbf{Y}}_J) > \beta\sqrt{BN_0}} i$ 
4:  $\tilde{\mathbf{P}}^{(0)} = \mathbf{I}_B - \mathbf{U}\mathbf{U}^\text{H}$  // cf. (16)
5:  $\tilde{\mathbf{S}}^{(0)} = [\mathbf{S}_T, (\hat{\mathbf{H}}^\text{H}\tilde{\mathbf{P}}^{(0)}\hat{\mathbf{H}} + N_0\mathbf{I}_U)^{-1}\hat{\mathbf{H}}^\text{H}\tilde{\mathbf{P}}^{(0)}\bar{\mathbf{Y}}_D]$ 
6: for  $t = 1$  to  $t_{\max}$  do
7:  $\tilde{\mathbf{E}}^{(t)} = [\bar{\mathbf{Y}}_T, \bar{\mathbf{Y}}_D](\mathbf{I}_K - \tilde{\mathbf{S}}^{(t-1)}\tilde{\mathbf{S}}^{(t-1)\dagger})$ 
8:  $\tilde{\mathbf{J}}^{(t)} = \text{APPROXSVD}(\tilde{\mathbf{E}}^{(t)}, \hat{I}^*)$  // cf. [36, Alg. 1]
9:  $\tilde{\mathbf{P}}^{(t)} = \mathbf{I}_B - \tilde{\mathbf{J}}^{(t)}(\tilde{\mathbf{J}}^{(t)})^\dagger$ 
10:  $\nabla f(\tilde{\mathbf{S}}^{(t-1)}) = -2([\bar{\mathbf{Y}}_T, \bar{\mathbf{Y}}_D]\tilde{\mathbf{S}}^{(t-1)\dagger})^\text{H}\tilde{\mathbf{P}}^{(t)}[\bar{\mathbf{Y}}_T, \bar{\mathbf{Y}}_D]$ 
    $\cdot (\mathbf{I}_K - \tilde{\mathbf{S}}^{(t-1)}\tilde{\mathbf{S}}^{(t-1)\dagger})$ 
11:  $\tilde{\mathbf{S}}^{(t)} = \text{prox}_g(\tilde{\mathbf{S}}^{(t-1)} - \tau^{(t)}\nabla f(\tilde{\mathbf{S}}^{(t-1)}); \tau^{(t)})$ 
12: end for
13: output:  $\tilde{\mathbf{S}}_{[T+1:K]}^{(t_{\max})}$ 
14: end function

```

---

The optimization problem to solve when combining MASH with MAED is

$$\min_{\substack{\tilde{\mathbf{P}} \in \mathcal{G}_{B-\hat{I}^*}(\mathbb{C}^B), \\ \hat{\mathbf{H}} \in \mathbb{C}^{B \times U}, \\ \tilde{\mathbf{S}}_D \in \mathcal{S}^{U \times \hat{D}}}} \|\tilde{\mathbf{P}}([\bar{\mathbf{Y}}_T, \bar{\mathbf{Y}}_D] - \hat{\mathbf{H}}[\mathbf{S}_T, \tilde{\mathbf{S}}_D])\|_{\text{F}}^2, \quad (31)$$

where  $\mathcal{G}_{B-\hat{I}^*}(\mathbb{C}^B)$  is as in (29). This problem can be transformed into an equivalent one that only depends on  $\tilde{\mathbf{P}}$  and  $\tilde{\mathbf{S}}_D$  (see [36, Sec. V-B]) and then can be approximately solved as in [36, Alg. 3]. As in the case of MASH-S, the robustness and speed of convergence can be improved if the algorithm is properly initialized using the information contained in  $\bar{\mathbf{Y}}_T$ , with the initial values of  $\tilde{\mathbf{P}}$  and  $\tilde{\mathbf{S}}_D$  being set using (16) and (22), respectively. We call the algorithm that results from this procedure MASH-M; see Algorithm 2. The proximal operator  $\text{prox}_g$  in line 11 of Algorithm 2 maps the first  $T$  columns of its input matrix to  $\mathbf{S}_T$  and for the remaining columns acts identical to the proximal operator of Algorithm 1.

## V. PRACTICAL EXTENSIONS AND MODIFICATIONS

### A. Individual Secrets: Reciprocal MASH

In the above description of MASH, all UEs were assumed to use the same secret  $\star$ . From a practical perspective, this is a

substantial drawback—the secret must be known by all UEs but the jammer must not know it.<sup>8</sup> We therefore propose *reciprocal MASH*, a variant of MASH that can be used with individual secrets, i.e., when every UE has its own secret known only to the BS and that UE. In future cellular standards, such as 6G, such secrets could be distributed to the UEs, e.g., through the subscriber identity module (SIM card) [39].

The basic idea behind reciprocal MASH is simple: The BS detects the data for each UE separately, and while it does so, it treats the other UEs as additional jamming interference. This strategy has two disadvantages. First, it increases the computational complexity at the BS, since the BS now has to solve  $U$  detection problems (even if these detection problems are only single-user problems). Second, treating the other  $U - 1$  UEs as additional interferers is suboptimal for detection and requires that the redundancy satisfies  $R \geq I^* + U - 1$  rather than just  $R \geq I^*$ . However, these disadvantages contrast with two significant advantages. The first advantage is the already discussed leap in practicality with regards to how the required secrets can be distributed to the UEs. The second advantage is the following: Since the BS regards all other UEs as additional interferers when detecting the data of any given UE, the UEs do not need to be synchronized to a joint schedule. This is advantageous for the following reason: To enable the joint synchronization of multiple UEs in existing cellular systems, synchronization signals have to be sent by the BS [40]. UEs can therefore be synchronized jointly—even for the uplink—only if they can correctly detect the synchronization signals in the downlink.<sup>9</sup> However, to the best of our knowledge, the only synchronization method that is resilient against universal jamming attacks is [41], which is a method for uplink synchronization, and which thus cannot synchronize multiple UEs jointly. Reciprocal MASH therefore enables multi-user MIMO even under the limitations of currently existing methods for jammer-resilient synchronization.

Reciprocal MASH works as follows: Let  $\mathbf{s}_{(u)}^T \in \mathbb{C}^{1 \times K}$  and  $\mathbf{C}_u = [\mathbf{C}_{\perp u}; \mathbf{C}_{\parallel u}] \in \mathbb{C}^{L \times L}$  be the transmit signal and the embedding matrix for the  $u$ th UE. Then the  $u$ th UE transmits

$$\mathbf{x}_{(u)}^T = \mathbf{s}_{(u)}^T \mathbf{C}_{\parallel u} \quad (32)$$

and the BS receives<sup>10</sup>

$$\mathbf{Y}_u = \mathbf{h}_u \mathbf{x}_{(u)}^T + \sum_{\substack{u'=1 \\ u' \neq u}}^U \mathbf{h}_{u'} \check{\mathbf{x}}_{(u')}^T + \mathbf{J} \mathbf{W}_u + \mathbf{N}_u. \quad (33)$$

Here,  $\check{\mathbf{x}}_{(u')}^T \in \mathbb{C}^{1 \times L}$  is the signal that the  $u'$ th UE transmits while the  $u$ th UE transmits  $\mathbf{x}_{(u)}^T$ . However, because we do not require that the UEs are jointly synchronized, it is generally not the case that  $\check{\mathbf{x}}_{(u')}^T = \mathbf{s}_{(u')}^T \mathbf{C}_{\parallel u'}$ . Instead,  $\check{\mathbf{x}}_{(u')}^T$  can overlap two of the  $u'$ th UE's transmit frames and thus may be any

contiguous length- $L$  subvector of  $[\mathbf{s}_{(u'),1}^T \mathbf{C}_{\parallel u'}, \mathbf{s}_{(u'),2}^T \mathbf{C}_{\parallel u'}]$ , where  $\mathbf{s}_{(u'),1}^T$  and  $\mathbf{s}_{(u'),2}^T$  are the  $u'$ th UE's messages which overlap with the current frame of the  $u$ th UE. By defining  $\check{\mathbf{X}}_{-u} \in \mathbb{C}^{(U-1) \times L}$  as the matrix whose rows consist of the row vectors  $\check{\mathbf{x}}_{(u')}$  for all  $u' \in [1 : U] \setminus \{u\}$ , and  $\check{\mathbf{H}}_{-u} \in \mathbb{C}^{B \times (U-1)}$  as the matrix whose columns consist of the channel vectors  $\mathbf{h}_{u'}$  for all  $u' \in [1 : U] \setminus \{u\}$ , we can rewrite (33) as

$$\begin{aligned} \mathbf{Y}_u &= \mathbf{h}_u \mathbf{x}_{(u)}^T + \underbrace{[\check{\mathbf{H}}_{-u} \quad \mathbf{J}]}_{\triangleq \check{\mathbf{J}}_u \in \mathbb{C}^{B \times (I+U-1)}} \cdot \underbrace{\begin{bmatrix} \check{\mathbf{X}}_{-u} \\ \mathbf{W}_u \end{bmatrix}}_{\triangleq \check{\mathbf{W}}_u \in \mathbb{C}^{(I+U-1) \times L}} + \mathbf{N}_u \quad (34) \\ &= \mathbf{h}_u \mathbf{x}_{(u)}^T + \check{\mathbf{J}}_u \check{\mathbf{W}}_u + \mathbf{N}_u. \quad (35) \end{aligned}$$

The BS can now raise the  $u$ th UE's message by multiplying  $\mathbf{Y}_u$  with  $\mathbf{C}_u^H$ , obtaining

$$\begin{aligned} \bar{\mathbf{Y}}_u &\triangleq \mathbf{Y}_u \mathbf{C}_u^H = \mathbf{h}_u \mathbf{s}_{(u)}^T \mathbf{C}_{\parallel u} \mathbf{C}_u^H + \check{\mathbf{J}}_u \underbrace{\check{\mathbf{W}}_u \mathbf{C}_u^H}_{\triangleq \check{\mathbf{W}}_u} + \underbrace{\mathbf{N} \mathbf{C}_u^H}_{\triangleq \bar{\mathbf{N}}_u} \quad (36) \\ &= \mathbf{h}_u [0_{1 \times R}, \mathbf{s}_{(u)}^T] + \check{\mathbf{J}}_u \bar{\mathbf{W}}_u + \bar{\mathbf{N}}_u, \quad (37) \end{aligned}$$

in direct analogy to (11). The raised receive signal for the  $u$ th UE corresponds thus to a single-user signal (which includes a length- $R$  jammer training period) that is contaminated by a  $(I + U - 1)$ -antenna barrage “jamming” signal.<sup>11</sup> The message of the  $u$ th UE can be detected using the methods of Section IV, and the entire process is repeated for every  $u \in [1 : U]$ .

## B. Efficient Embedding/Raising Transforms

For Theorem 1 in Section IV, we have assumed that the embedding matrix  $\mathbf{C} = f(\clubsuit)$  is Haar distributed, i.e., uniformly distributed over the set of unitary  $L \times L$  matrices. A Haar distributed matrix can be obtained as follows: Draw a matrix with i.i.d.  $\mathcal{CN}(0, 1)$  entries and compute its QR-decomposition using the Gram-Schmidt procedure. The resulting  $\mathbf{Q}$ -matrix is Haar distributed [32, Sec. 1.2]. Unfortunately, this approach is not practical as it exhibits high computational complexity. If  $f$  is a deterministic function that converts the secret  $\clubsuit$  first into a Gaussian matrix and from there into a Haar matrix, then  $\clubsuit$  needs to contain an infinite amount of entropy. Furthermore, to prevent the jammer from learning the matrix  $\mathbf{C}$  over time, this Haar distributed transform matrix should be replaced frequently (ideally after every use). But computing the QR-decomposition has a complexity of  $O(L^3)$ , so the computational cost of doing so would be prohibitive.

To address these two issues, we propose to use transform matrices for embedding and raising that are approximately Haar distributed. Specifically, we approximate a Haar matrix as

$$\mathbf{C} = \mathbf{F} \mathbf{D}_1 \mathbf{F} \mathbf{D}_2 \mathbf{F}, \quad (38)$$

where  $\mathbf{D}_1$  and  $\mathbf{D}_2$  are diagonal random matrices that have i.i.d.  $\text{Unif}\{-1, +1\}$  diagonal entries (i.e., diagonal matrices whose diagonals are Rademacher distributed), and where  $\mathbf{F}$  is either the discrete fourier transform (DFT) matrix or the Walsh-Hadamard matrix. Such matrices approximate Haar matrices in the sense that, like Haar matrices, they are restricted isometry

<sup>11</sup>The effective rank of the interference  $\check{\mathbf{J}}_u \bar{\mathbf{W}}_u$  may be less than  $I + U - 1$  in the same way that  $I^*$  may be smaller than  $I$ , see Section III.

<sup>8</sup>As the saying goes: “Two can keep a secret if one of them is dead.”

<sup>9</sup>Jammer mitigation in the downlink is an even more formidable problem than in the uplink, because UEs may not have more antennas than a jammer. However, in many scenarios (e.g., internet of things or sensor networks), it may already be beneficial if a unidirectional communication link can be established.

<sup>10</sup>The receive signal  $\mathbf{Y}_u$  depends on the index  $u$  of the considered UE because the BS is synchronized to the frame alignment of the  $u$ th UE, which may differ from the frame alignment of the other UEs. If all UEs are synchronized to the same frame alignment, then  $\mathbf{Y}_u$  does not depend on  $u$ .

TABLE I  
COMPUTATIONAL COMPLEXITY OF EMBEDDING AND RAISING

	Exact Haar	Approximate Haar
Construction of $\mathbf{C}^a$	$O(L^3)$	0
Embedding (per UE)	$O(LK)$	$O(L \log L)$
Raising	$O(BL^2)$	$O(BL \log L)$

<sup>a</sup>The impact on complexity of constructing a pseudorandom Gaussian matrix or a Rademacher vector is neglected.

property (RIP) optimal in certain regimes [42]. Concatenations of Walsh-Hadamard and random Rademacher diagonal matrices have also been used to approximate random rotations<sup>12</sup> in [43]. Note that using a matrix  $\mathbf{C}$  as in (38) for embedding and raising does not even require  $\mathbf{C}$  to be computed explicitly. Instead, multiplying with  $\mathbf{C}_{\parallel}$  (embedding) and with  $\mathbf{C}^H$  (raising) can be implemented by a series of fast Fourier/Hadamard transforms that alternates with appropriate element-wise sign changes. Using fast transforms also reduces the computational complexity of raising/embedding itself; see Table I.

## VI. EXPERIMENTAL EVALUATION

### A. Simulation Setup

We simulate the uplink of a massive multi-user (MU) MIMO system with  $B = 64$  antennas at the BS and  $U = 16$  UEs. The channel vectors are generated using QuaDRiGa [46] with the 3GPP 38.901 urban macrocellular (UMa) channel model [47]. The carrier frequency is 2GHz and the BS antennas are arranged as a uniform linear array (ULA) with half-wavelength spacing. The UEs and the jammer are distributed randomly at distances from 10 m to 250 m in a  $120^\circ$  angular sector in front of the BS, with a minimum angular separation of  $1^\circ$  between any two UEs as well as between the jammer and any UE. The jammer can be a single- or a multi-antenna jammer (see Section VI-C). The antennas of multi-antenna jammers are arranged as a half-wavelength ULA that is facing the BS's direction. All antennas are assumed to be omnidirectional and the UEs are assumed to use  $\pm 3$  dB power control.

As in Section IV, we consider coherent data transmission. The framelength is  $L = 100$ , and is divided into a redundancy of  $R = 16$ ,  $T = 16$  pilot samples, and  $L - R - T = 68$  data samples. The transmit constellation  $\mathcal{S}$  is QPSK, and the pilots  $\mathbf{S}_T$  are chosen as a  $16 \times 16$  Hadamard matrix (normalized to unit symbol energy). We characterize the strength of the jammer interference relative to the strength of the average UE via

$$\rho \triangleq \frac{\|\mathbf{J}\mathbf{W}\|_{\mathbb{F}}^2}{\frac{1}{U} \mathbb{E}_{\mathbf{S}}[\|\mathbf{H}\mathbf{X}\|_{\mathbb{F}}^2]}. \quad (39)$$

The average signal-to-noise ratio (SNR) is defined as

$$\text{SNR} \triangleq \frac{\mathbb{E}_{\mathbf{S}}[\|\mathbf{H}\mathbf{X}\|_{\mathbb{F}}^2]}{\mathbb{E}_{\mathbf{N}}[\|\mathbf{N}\|_{\mathbb{F}}^2]}. \quad (40)$$

<sup>12</sup>The random "rotations" in [43] are random Gaussian matrices that are only approximately unitary, but that behave similarly to Haar matrices [44], [45].

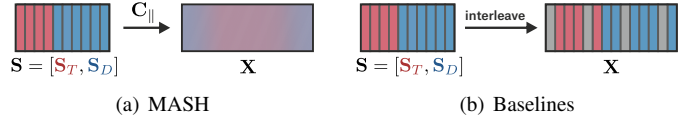


Fig. 4. MASH (left) maps a length- $K$  signal  $\mathbf{S} = [\mathbf{S}_T, \mathbf{S}_D]$  to a length- $L$  signal  $\mathbf{X}$  by multiplying with  $\mathbf{C}_{\parallel}$ . The baselines (right) map a length- $K$  signal  $\mathbf{S} = [\mathbf{S}_T, \mathbf{S}_D]$  to a length- $L$  signal by interleaving it with evenly spread zero-symbols (shown in gray) that serve as jammer training period. For the baselines, we denote the receive samples corresponding to the jammer training period, pilot phase, and data phase as  $\mathbf{Y}_J$ ,  $\mathbf{Y}_T$  and  $\mathbf{Y}_D$ , respectively. These matrices are the non-MASH counterparts of  $\hat{\mathbf{Y}}_J$ ,  $\hat{\mathbf{Y}}_T$  and  $\hat{\mathbf{Y}}_D$  in (12)-(14).

As performance metrics, we use uncoded bit error rate (BER) as well as the modulation error ratio (MER)

$$\text{MER} \triangleq \frac{\mathbb{E}[\|\hat{\mathbf{S}}_D - \mathbf{S}_D\|_{\mathbb{F}}]}{\mathbb{E}[\|\mathbf{S}_D\|_{\mathbb{F}}]}, \quad (41)$$

which is a surrogate for error vector magnitude (EVM) [48]. Recall that the 3GPP 5G NR technical specification requires an EVM below 17.5% [48, Tbl. 6.5.2.2-1] for QPSK transmission.

### B. Methods and Baselines

We compare MASH against baselines which, instead of embedding the pilots and data symbols in a secret higher-dimensional space, transmit them in the conventional way, but interleave them with  $R$  zero-symbols that are evenly distributed over the frame and serve as jammer training period (cf. Fig. 4).

**MASH-L:** This receiver operates as described in Sec. IV-B.

**MASH-M:** This receiver operates as described in Sec. IV-C and uses  $t_{\max} = 10$  algorithm iterations.

**JL:** This baseline operates on a jammerless (JL) system. The transmitter operates as depicted in Fig. 4(b). The receiver ignores the receive samples of the jammer training period and performs LS channel estimation and LMMSE data detection.

**Unmitigated (Unm.):** This baseline does not mitigate the jammer. The transmitter operates as depicted in Fig. 4(b). The receiver ignores the receive samples of the jammer training period and performs LS channel estimation and LMMSE data detection as one would in a jammerless environment.

**LMMSE:** This baseline is identical to MASH-L, except that it does not use secret subspace embeddings. The transmitter operates as depicted in Fig. 4(b). The receiver estimates the jammer's spatial covariance matrix using the receive samples  $\mathbf{Y}_J$  from the training period,  $\hat{\mathbf{C}}_J = \frac{1}{R} \mathbf{Y}_J \mathbf{Y}_J^H$ , and then performs jammer-mitigating channel estimation and data detection analogous to (24) and (25).

**MAED:** This baseline is identical to MASH-M, except that it does not use secret subspace embeddings. The transmitter operates as depicted in Fig. 4(b), and the receiver operates as in Algorithm 2, except that its inputs are  $\mathbf{Y}_J$ ,  $\mathbf{Y}_T$ ,  $\mathbf{Y}_D$  instead of  $\hat{\mathbf{Y}}_J$ ,  $\hat{\mathbf{Y}}_T$ ,  $\hat{\mathbf{Y}}_D$ . It uses  $t_{\max} = 10$  algorithm iterations as well.

For the sake of figure readability, we omit the orthogonal projection variant of Section IV-A from our experiments, which performs similarly as MASH-L. None of the methods is given a priori knowledge about the dimension  $I^*$  of the interference space. The methods that require such knowledge estimate  $I^*$  as the number of the singular values of  $\hat{\mathbf{Y}}_J$  (MASH-M) or of  $\mathbf{Y}_J$  (MAED) that exceed  $2\sqrt{BN_0}$ ; cf. (15).



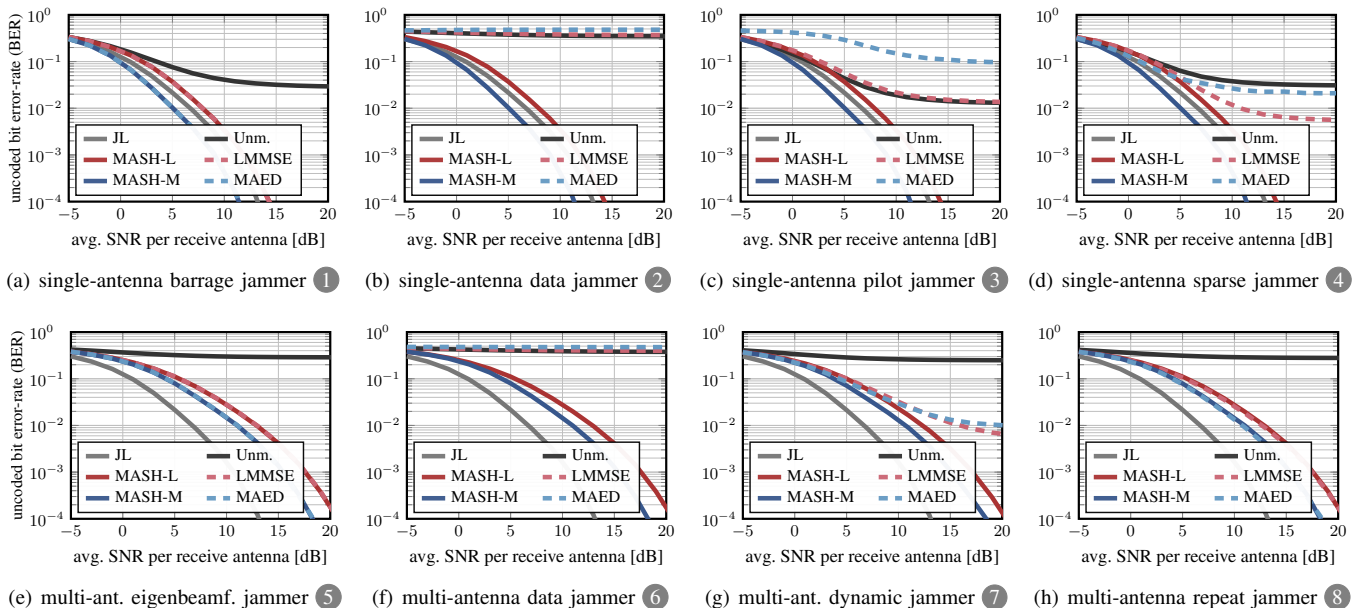


Fig. 5. Bit error rate (BER) performance of the different MASH receivers and baselines for eight different types of jammers.

### C. Jammer Types

The transmit signals of all jammers are normalized to  $\rho = 30$  dB. All multi-antenna jammers have  $I = 10$  antennas.

① *Single-antenna barrage jammer*: This jammer transmits i.i.d.  $\mathcal{CN}(0, 1)$  symbols for all samples.

② *Single-antenna data jammer*: This jammer transmits i.i.d.  $\mathcal{CN}(0, 1)$  symbols in all samples in which the UEs transmit data symbols<sup>13</sup> and is idle for all other samples.

③ *Single-antenna pilot jammer*: This jammer transmits i.i.d.  $\mathcal{CN}(0, 1)$  symbols during the UE pilot transmission period and is idle for all other samples.

④ *Single-antenna sparse jammer*: This jammer transmits i.i.d.  $\mathcal{CN}(0, 1)$  symbols in a fraction of  $\alpha = 0.1$  of non-contiguous randomly selected samples and is idle for all other samples.

⑤ *Multi-antenna eigenbeamforming jammer*: This jammer is assumed to have full knowledge of  $\mathbf{J} = \mathbf{U}\mathbf{\Sigma}\mathbf{V}^H$  and uses eigenbeamforming to transmit  $\mathbf{W} = \mathbf{V}\tilde{\mathbf{W}}$ , where the entries of  $\tilde{\mathbf{W}}$  are i.i.d.  $\mathcal{CN}(0, 1)$ . According to Definition 1, this jammer is a barrage jammer.

⑥ *Multi-antenna data jammer*: This jammer transmits i.i.d. random vectors  $\mathbf{w}_k \sim \mathcal{CN}(\mathbf{0}, \mathbf{I}_I)$  for all samples  $k$  in which the UEs transmit data symbols and is idle in all other samples.

⑦ *Multi-antenna dynamic-beamforming jammer*: At any given instance  $k$ , this jammer uses only a subset of its antennas, but it uses dynamic beamforming to change its antennas over time. Specifically, its time- $k$  beamforming matrix  $\mathbf{A}_k$  contains at most eight non-zero rows (the index set of these rows is generated uniform at random) whose entries are drawn i.i.d. at random from  $\mathcal{CN}(0, 1)$ . The matrix  $\mathbf{A}_{k+1}$  is equal to  $\mathbf{A}_k$  with probability 0.95, and with probability 0.05, it is redrawn at random. The vectors  $\tilde{\mathbf{w}}_k$  are drawn from  $\mathcal{CN}(\mathbf{0}, \mathbf{I}_I)$  for all  $k$ .

<sup>13</sup>This refers to the samples of the baseline methods as in Fig. 4(b). The subspace embeddings of MASH entail that data symbols are not transmitted during specific samples; cf. Fig. 4(a). The same applies to jammers ③ and ⑥.

⑧ *Multi-antenna repeat jammer*: This jammer is assumed to have sensing capabilities that allow it to perfectly detect the UE transmit signal. The jammer then simply repeats the transmit signal  $\mathbf{X}_{(1:i)}$  (cf. (7)) of the first  $I$  UEs with a delay of one sample, i.e.,  $\mathbf{W} = [\mathbf{0}_{I \times 1}, \mathbf{X}_{(1:I), [1:L-1]}]$ .

### D. Results

The results in Fig. 5 and Fig. 6 show that MASH mitigates *all* jammers under consideration, and so confirm the universality of MASH. We start by discussing the BER results of Fig. 5.

When facing the single-antenna barrage jammer in Fig. 5(a), MASH-L and MASH-M have exactly the same performance as their non-MASH counterparts LMMSE and MAED. This is expected, since transforming a barrage jammer into its equivalent barrage jammer changes nothing. LMMSE and MASH-L perform close to the JL baseline. MAED and MASH-M use a more complex, nonlinear JED-based data detector [29], and so are able to perform even better than the JL baseline.

For the more sophisticated single-antenna jammers, however, the picture changes (Fig. 5(c)–Fig. 5(d)): LMMSE performs poorly against all of them, since the training receive matrix  $\mathbf{Y}_J$  does not (or not necessarily, in the case of the sparse jammer ④) contain samples in which the jammer is transmitting. MAED performs comparably bad.<sup>14</sup> However, MASH-L and MASH-M transform all these jammers into their equivalent barrage jammers and thus—as predicted by theory—have *exactly* the same performance as they do for the barrage jammer in Fig. 5(a).

For the multi-antenna jammers, we observe the following (Fig. 5(e)–Fig. 5(h)): The eigenbeamforming jammer in Fig. 5(e) is also a barrage jammer (even if it uses beamforming). So, as in Fig. 5(a), the MASH methods have exactly the same performance as their non-MASH counterparts. However, since

<sup>14</sup>In principle, MAED would be able to mitigate such jammers—if given knowledge of  $\mathbf{I}^*$  [30], [36]. Here, the problem is that MAED’s estimate of  $\mathbf{I}^*$  will (wrongly) be zero whenever  $\mathbf{Y}_J$  contains no jammer samples.

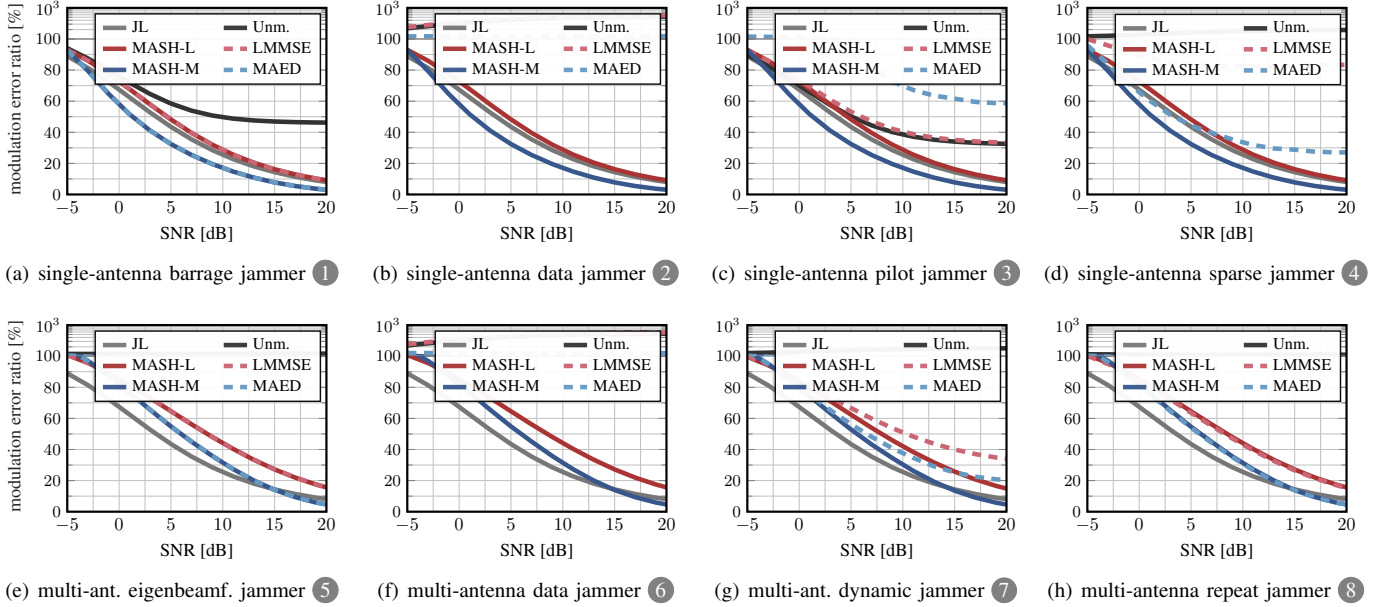


Fig. 6. Modulation error ratio (MER) performance of different MASH receivers and baselines for eight types of jammers. Note that the MER can exceed 100% when mitigation fails. Note also that the  $y$ -axis is scaled linearly between 0 and 100, and logarithmically between 100 and 1000.

the jammer now occupies 10 spatial dimensions (instead of 1) that need to be suppressed, the performance gap between the mitigation methods and the JL baseline (which does not have to suppress any dimensions) is larger than in Fig. 5(a) (the JMD methods MASH-M and MAED now perform worse than JL in spite of their nonlinear data detectors). For the multi-antenna data jammers in Fig. 5(f), the non-MASH baselines fail spectacularly, while the MASH methods still have the same performance as for the multi-antenna barrage jammer in Fig. 5(e). Similar observations apply to the dynamic-beamforming jammer in Fig. 5(g), except that here, the non-MASH baselines can estimate parts of the interference subspace (or all of it, if they are lucky) during the training period and, thus, fare somewhat better. Finally, the repeat jammer in Fig. 5(h) behaves functionally almost like a barrage jammer and is successfully mitigated by all mitigation methods (note that the jammer transmits different signals for the MASH and the non-MASH methods). This experiment demonstrates that not even sneaky repeat attacks are able to overcome MASH. This was to be expected, of course, since  $\text{row}(\mathbf{C}_{\parallel})$  is, in general, not closed under cyclic shifts of the rows of  $\mathbf{C}_{\parallel}$ . (However, to prevent repeat attacks against MASH on the level of entire frames, the transmitters and receiver should update the matrix  $\mathbf{C}$  according to a pseudo-random sequence after every transmission frame.)

The MER results in Fig. 6 show strong agreement with the BER results in Fig. 5. The *only* observable difference is that the nonlinear methods MAED/MASH-M perform slightly better compared the linear methods JL/LMMSE/MASH-L in terms of MER than in terms of BER. (This is due to the data symbol prior of MAED/MASH-M, which pulls symbol estimates to constellation points and so achieves lower Euclidean error than linear detection even when the underlying decoded bits are the same.) Even so, the results of Fig. 6 agree with those of Fig. 5: the MASH methods are the only ones that successfully mitigate *all* types of jammers, while the traditional baselines

that do not use subspace embeddings fail in many of the cases.

### E. Evaluation of Reciprocal MASH

Next, we evaluate the performance of reciprocal MASH from Section V-A. For this, the setup is exactly as in Section VI-A, except that we now consider only  $U = 8$  UEs—for reciprocal MASH, the performance decreases considerably as  $U + I^*$  approaches  $R$ . Since the performance of MASH vis-à-vis the state of the art has been evaluated in Section VI-D, we now only compare reciprocal and non-reciprocal MASH. For reciprocal MASH, the following two receivers are considered:

**Recip. MASH-L:** This receiver uses reciprocal MASH as in Section V-A with an LMMSE receiver as in Section IV-B.

**Recip. MASH-M:** This receiver uses reciprocal MASH as in Section V-A with an LMMSE receiver as in Section IV-C. However, in contrast to MASH-M as described in Section VI-B, the reciprocal variant uses only  $t_{\max} = 5$  iterations per single-UE detection problem, and it estimates the interference subspace dimension as the number of singular values (averaged over  $u = 1, \dots, U$ ) of  $\bar{\mathbf{Y}}_{J,u}$  that exceed  $\sqrt{BN_0}$  (instead of  $2\sqrt{BN_0}$ ).<sup>15</sup>

Noting the close agreement between BER and MER, we evaluate only the BER to assess the performance. We still consider all types of jammers 1–8 (with jamming power  $\rho = 30$  dB), but the multi-antenna jammers now have only  $I = 6$  antennas (to ensure that  $R \geq I + U - 1$  holds, since  $R = 16$ ).

The results are shown in Fig. 7. As mentioned in Section V-A, treating the other  $U - 1$  UEs as additional interferers is suboptimal for detection, and there is a corresponding performance loss for reciprocal MASH compared to regular (“common”) MASH. For the single-antenna jammers

<sup>15</sup>When, as in this experiment, all UEs are jointly synchronized, then the dimension of the interference subspace is the same for all UE detection problems. Hence, the estimation of this dimension can be improved by considering the observations from all UEs jointly.

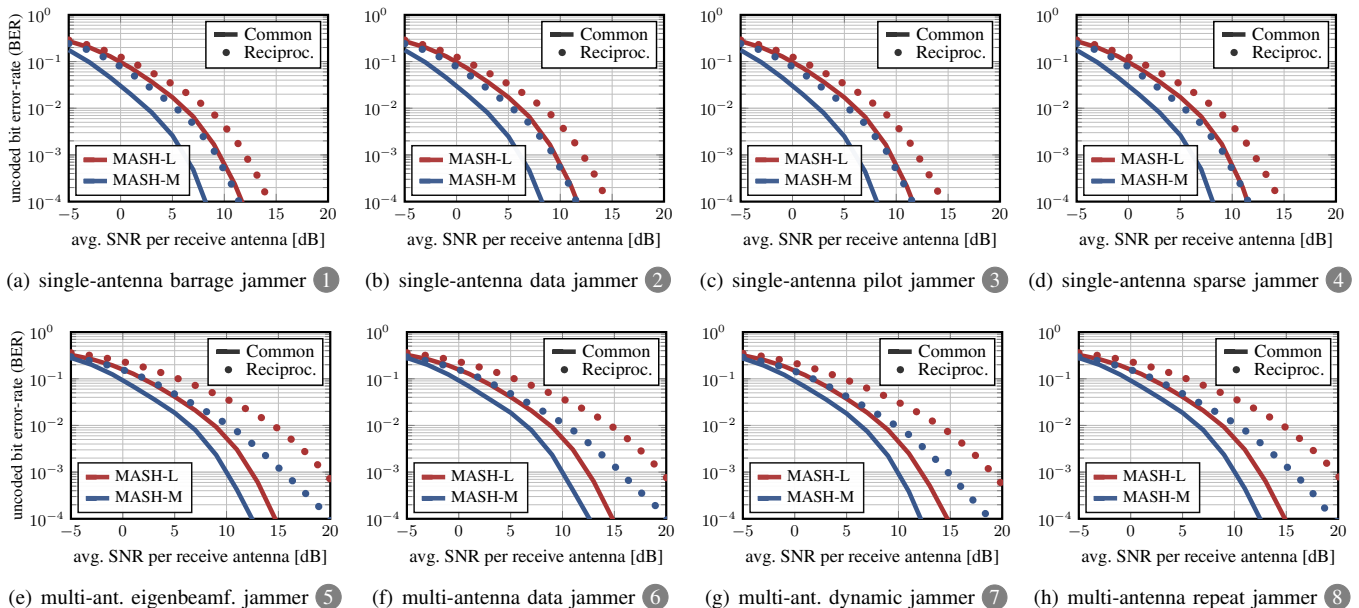


Fig. 7. Bit error rate (BER) performance comparison between MASH with a common secret shared between the BS and all UEs (Common) and reciprocal MASH.

(Fig. 7(a)–Fig. 7(d)), reciprocal MASH-L and MASH-M lose roughly 3 dB and 4 dB in SNR (at a BER of  $10^{-3}$ ) compared to their non-reciprocal counterparts, respectively. For the multi-antenna jammers (Fig. 7(e)–Fig. 7(h)), these losses become more pronounced since the dimension  $I^* + U - 1$  of the “interference” subspace (for reciprocal MASH) approaches the redundancy  $R$ . Note, however, that reciprocal MASH does not exhibit any signs of an error floor. The performance gap could be narrowed by increasing the redundancy  $R$ , at the expense of reduced number of data symbols per transmission frame.

#### F. Evaluation of Efficient Embedding/Raising Transforms

Finally, we evaluate the performance of the efficient embedding/raising transforms from Section V-B, specifically the version based on the Walsh-Hadamard matrix. The setup is again as in Section VI-A, except that the frame length is now  $L = 96$  (instead of  $L = 100$ ), resulting in  $L - R - T = 64$  data samples. The reason for this change is that there exists no Walsh-Hadamard matrix of size  $100 \times 100$ , but there exists one of size  $96 \times 96$ . We consider the following two new methods:

**Approx. MASH-L:** This method uses the Walsh-Hadamard-based matrix from Section V-B for embedding and raising. The receiver operates like the MASH-L receiver from Section VI-B.

**Approx. MASH-M:** This method uses the Walsh-Hadamard-based matrix from Section V-B for embedding and raising. The receiver operates like the MASH-M receiver from Section VI-B.

We compare these two methods with their Haar distributed counterparts from Section VI-B. The BER results for all types of jammers ①–⑧ are depicted in Fig. 8. For the single-antenna jammers, there is no discernible difference between MASH based on exact Haar matrices and MASH based on approximate Haar matrices (Fig. 8(a)–Fig. 8(d)). Also for the multi-antenna jammers, the performance difference is less than 0.5 dB in all cases. This indicates that the efficient embedding/raising transforms succeed in approximating the behavior of Haar-based transform matrices for the purposes of MASH. Also

note that, for barrage jammers, the performance is exactly identical, since barrage jammers are statistically invariant to unitary transforms (which includes Haar matrices as well as the approximate transforms of Section V-B), see Fig. 8(a), Fig. 8(e).

## VII. CONCLUSIONS

We have provided a mathematical definition to capture the essence of the notion of barrage jammers, which are easy to mitigate using multi-antenna spatial filtering. For single-antenna barrage jammers, we have also derived a fundamental new result in Proposition 1, which *proves* that it is easy to mitigate them using MIMO processing. Furthermore, we have proposed MASH, a novel method in which the transmitters embed their signals in a secret temporal subspace out of which the receiver raises them, thereby provably (cf. Theorem 1) transforming *any* jammer into a barrage jammer. Considering a massive MU-MIMO uplink example scenario, we have provided three concrete variations of MASH with different performance-complexity tradeoffs. Furthermore, we have proposed a way to remedy the difficulty of supplying a common secret to multiple UEs (while ensuring that the jammer does not learn about the secret) by proposing *reciprocal* MASH. In reciprocal MASH, each UE uses its own secret (known only to the BS and that UE), while the BS detects the data of the different UEs and treats the respective other UEs as additional interference. We then have suggested the use of transform matrices that are approximately Haar distributed, but that reduce both the computational complexity of the legitimate transceivers as well as the required entropy of the shared random secret. Finally, the efficacy of MASH in all its variants, and against many conceivable types of jammers, has been demonstrated using extensive numerical simulation results.

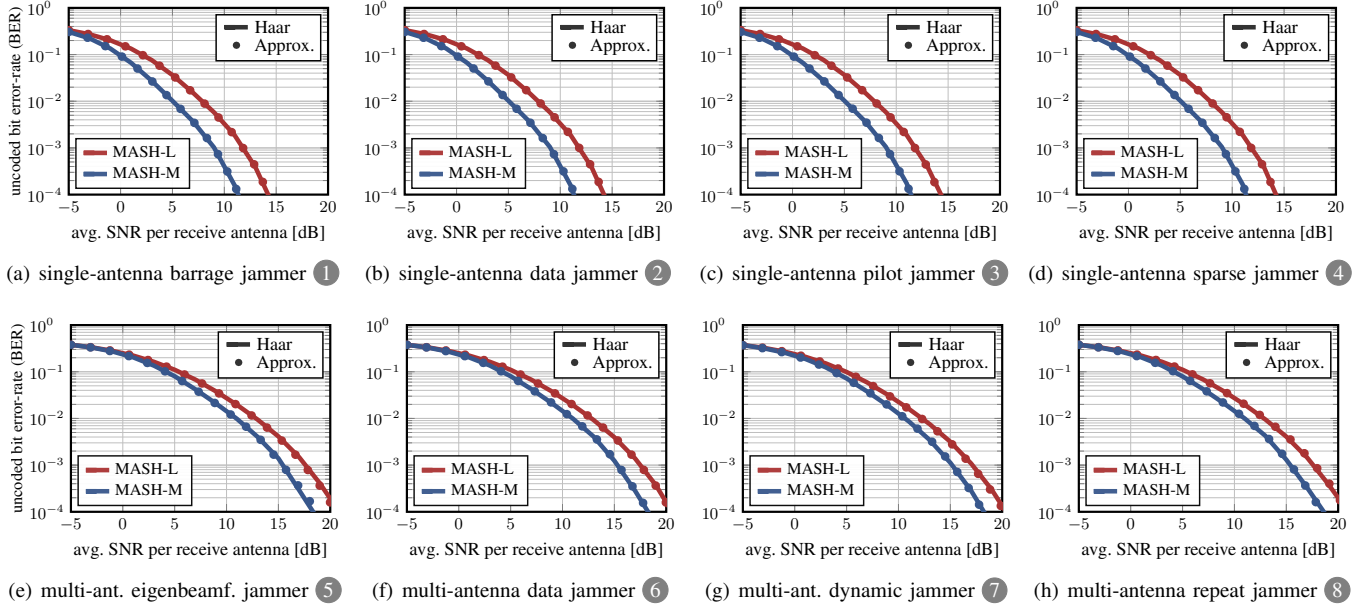


Fig. 8. Bit error rate (BER) performance comparison between MASH with Haar distributed transform matrices and with approximately Haar distributed transform matrices (Approx.).

## APPENDIX A PROOF OF PROPOSITION 1

The proof consists of two cases that are considered. In one case, we assume that the noise  $\mathbf{N}$  satisfies

$$\|\mathbf{N}_{[1:R]}\|^2 \leq \alpha^{-1} \left(\frac{3}{2} - \sqrt{2}\right) \|\mathbf{j}\|_2^2 \|\mathbf{w}\|_2^2 \frac{L}{R}, \quad (42)$$

and in the other case, we assume the reverse. We start with the case where (42) holds. The compact SVD of the interference  $\mathbf{j}\mathbf{w}^T$  is  $\mathbf{u}\sigma\mathbf{v}^H$ , with  $\sigma = \|\mathbf{j}\|_2 \|\mathbf{w}\|_2$ , and with  $\mathbf{v}$  being uniformly distributed over the complex  $L$ -dimensional unit sphere (since the jammer is a barrage jammer). We may therefore write

$$(\mathbf{j}\mathbf{w}^T + \mathbf{N})_{[1:R]} = \mathbf{u}\sigma(\mathbf{v}^H)_{[1:R]} + \mathbf{N}_{[1:R]} \quad (43)$$

$$= \mathbf{u}(\sigma\|\mathbf{v}_{[1:R]}\|_2) \frac{(\mathbf{v}^H)_{[1:R]}}{\|\mathbf{v}_{[1:R]}\|_2} + \mathbf{N}_{[1:R]}. \quad (44)$$

From [49, Lem. 2.2], it follows that, for any  $\alpha > 1$ ,

$$\|\mathbf{v}_{[1:R]}\|_2 > \sqrt{\frac{R}{\alpha L}} \quad (45)$$

holds with probability at least

$$1 - \alpha^{-R} \left(\frac{L-R/\alpha}{L-R}\right)^{L-R}. \quad (46)$$

For the remainder of this first case, we condition on this event. Wedin's  $\sin \Theta$  theorem [50, Thm. 2.9] implies that if  $\|\mathbf{N}_{[1:R]}\| \leq \left(1 - \frac{1}{\sqrt{2}}\right) \sigma\|\mathbf{v}_{[1:R]}\|_2$ —which is implied by (42)—then the estimate  $\mathbf{u}_1$  of the jammer subspace  $\mathbf{u}$  satisfies

$$\|\mathbf{u}_1\mathbf{u}_1^H - \mathbf{u}\mathbf{u}^H\| \leq \frac{2\|\mathbf{N}_{[1:R]}\|}{\sigma\|\mathbf{v}_{[1:R]}\|_2} < \frac{2\|\mathbf{N}_{[1:R]}\|}{\|\mathbf{j}\|_2 \|\mathbf{w}\|_2 \sqrt{R/(\alpha L)}}. \quad (47)$$

We can therefore bound the square root of the residual jammer interference energy after the projection as

$$\|\mathbf{P}\mathbf{j}\mathbf{w}^T\|_F = \|(\mathbf{I}_B - \mathbf{u}_1\mathbf{u}_1^H)\mathbf{j}\|_2 \|\mathbf{w}\|_2 \quad (48)$$

$$= \|(\mathbf{I}_B - \mathbf{u}\mathbf{u}^H + \mathbf{u}\mathbf{u}^H - \mathbf{u}_1\mathbf{u}_1^H)\mathbf{j}\|_2 \|\mathbf{w}\|_2 \quad (49)$$

$$\leq \underbrace{\|(\mathbf{I}_B - \mathbf{u}\mathbf{u}^H)\mathbf{j}\|_2}_{=0} \|\mathbf{w}\|_2 + \|(\mathbf{u}\mathbf{u}^H - \mathbf{u}_1\mathbf{u}_1^H)\mathbf{j}\|_2 \|\mathbf{w}\|_2 \quad (50)$$

$$\leq \|\mathbf{u}_1\mathbf{u}_1^H - \mathbf{u}\mathbf{u}^H\| \|\mathbf{j}\|_2 \|\mathbf{w}\|_2 \quad (51)$$

$$\leq \frac{2\|\mathbf{N}_{[1:R]}\|}{\|\mathbf{j}\|_2 \|\mathbf{w}\|_2 \sqrt{R/(\alpha L)}} \|\mathbf{j}\|_2 \|\mathbf{w}\|_2 \quad (52)$$

$$= 2\|\mathbf{N}_{[1:R]}\| \sqrt{\frac{\alpha L}{R}}, \quad (53)$$

where in (50) we used the triangle inequality and the fact that  $(\mathbf{I}_B - \mathbf{u}\mathbf{u}^H)\mathbf{j} = \mathbf{0}$  since  $\mathbf{I}_B - \mathbf{u}\mathbf{u}^H$  is the projection onto the orthogonal complement of  $\text{col}(\mathbf{j})$ , and where in (52) we used (47). By taking the square, we therefore get

$$\|\mathbf{P}\mathbf{j}\mathbf{w}^T\|_F^2 \leq \alpha 4 \|\mathbf{N}_{[1:R]}\|^2 \frac{L}{R} \quad (54)$$

In the second case, we assume that (42) does *not* hold. In that case, we can bound the residual jammer interference energy as

$$\|\mathbf{P}\mathbf{j}\mathbf{w}^T\|_F^2 \leq \|\mathbf{j}\mathbf{w}^T\|_F^2 = \|\mathbf{j}\|_2^2 \|\mathbf{w}\|_2^2 \quad (55)$$

$$< \alpha \frac{1}{\frac{3}{2} - \sqrt{2}} \|\mathbf{N}_{[1:R]}\|^2 \frac{L}{R}, \quad (56)$$

where in (55) we use the fact that projections are contractions, and where in (56) we use that (42) does not hold.

In summary, we get that if (42) holds, then (54) holds with probability at least (46); and if (42) does not hold, then (56) holds with probability 1. By taking the weaker bounds of both cases, it follows that

$$\|\mathbf{P}\mathbf{j}\mathbf{w}^T\|_F^2 \leq \alpha \frac{1}{\frac{3}{2} - \sqrt{2}} \|\mathbf{N}_{[1:R]}\|^2 \frac{L}{R} \quad (57)$$

holds with probability at least (46), regardless of whether (42) holds. The result follows dividing both sides by  $L$ , and by using the facts  $\|\mathbf{N}_{[1:R]}\|^2 \leq \|\mathbf{N}_{[1:R]}\|_F^2$  and  $\frac{1}{\frac{3}{2} - \sqrt{2}} < 12$ .  $\color{red}{\blacklozenge}$



APPENDIX B  
PROOF OF THEOREM 1

We rewrite the compact SVD of  $\mathbf{J}\mathbf{W} = \mathbf{U}\mathbf{\Sigma}\mathbf{V}^H$  as a full SVD  $\mathbf{J}\mathbf{W} = \mathbf{U}\mathbf{\Sigma}\mathbf{V}^H$  with  $\mathbf{U} \in \mathbb{C}^{B \times B}$ ,  $\mathbf{\Sigma} \in \mathbb{C}^{B \times L}$ , and  $\mathbf{V} \in \mathbb{C}^{L \times L}$ . We then have  $\mathbf{J}\mathbf{W}\mathbf{C}^H = \mathbf{U}\mathbf{\Sigma}(\mathbf{C}\mathbf{V})^H$ . Since  $\mathbf{C}$  is Haar distributed, so is  $\mathbf{C}\mathbf{V}$  [32, Thm. 1.4]. The compact SVD of  $\mathbf{J}\mathbf{W}\mathbf{C}^H = \bar{\mathbf{U}}\bar{\mathbf{\Sigma}}\bar{\mathbf{V}}^H$  is  $\bar{\mathbf{U}} = \mathbf{U}_{[1:I^*]} = \mathbf{U}$ ,  $\bar{\mathbf{\Sigma}} = \mathbf{\Sigma}_{(1:I^*),[1:I^*]} = \mathbf{\Sigma}$ , which implies  $\bar{\boldsymbol{\sigma}} = \boldsymbol{\sigma}$ , and  $\bar{\mathbf{V}} = (\mathbf{C}\mathbf{V})_{[1:I^*]}$ . Since  $\mathbf{C}\mathbf{V}$  is Haar distributed, the columns of  $\bar{\mathbf{V}}$  are distributed uniformly over the complex  $L$ -dimensional sphere.  $\color{red}{\blacklozenge}$

REFERENCES

- [1] G. Marti and C. Studer, "Universal MIMO jammer mitigation via secret temporal subspace embeddings," pp. 1–8, Oct 2023.
- [2] E. Dahlman, S. Parkvall, and J. Skold, *5G NR: The next generation wireless access technology*. Academic Press, 2020.
- [3] M. Lichtman, R. Rao, V. Marojevic, J. Reed, and R. P. Jover, "5G NR jamming, spoofing, and sniffing: Threat assessment and mitigation," in *Proc. IEEE Int. Conf. Commun. Workshop (ICCW)*, May 2018, pp. 1–6.
- [4] F. Girke, F. Kurtz, N. Dorsch, and C. Wietfeld, "Towards resilient 5G: Lessons learned from experimental evaluations of LTE uplink jamming," in *IEEE Int. Conf. Commun. Workshop (ICCW)*, May 2019, pp. 1–6.
- [5] 5G Threat Model Working Panel, "Potential threat vectors to 5G infrastructure," *CISA, NSA, and DNI*, May 2021.
- [6] G. Guanella, "Means for and method of secret signaling," U.S. Patent 2405500, Aug. 1946.
- [7] U. Madhow and M. L. Honig, "MMSE interference suppression for direct-sequence spread-spectrum CDMA," *IEEE Trans. Commun.*, vol. 42, no. 12, pp. 3178–3188, Dec. 1994.
- [8] N. Tesla, "System of signaling," U.S. Patent 725605A, Apr. 1903.
- [9] W. Stark, "Coding for frequency-hopped spread-spectrum communication with partial-band interference-part i: capacity and cutoff rate," vol. 33, no. 10, pp. 1036–1044, 1985.
- [10] Y. Léost, M. Abdi, R. Richter, and M. Jeschke, "Interference rejection combining in LTE networks," *Bell Labs Tech. J.*, vol. 17, no. 1, pp. 25–50, Jun. 2012.
- [11] R. Miller and W. Trappe, "Subverting MIMO wireless systems by jamming the channel estimation procedure," in *Proc. ACM Conf. Wireless Netw. Security*, Mar. 2010, pp. 19–24.
- [12] M. Lichtman, J. D. Poston, S. Amuru, C. Shahriar, T. C. Clancy, R. M. Buehrer, and J. H. Reed, "A communications jamming taxonomy," *IEEE Security & Privacy*, vol. 14, no. 1, pp. 47–54, 2016.
- [13] H. Pirayesh and H. Zeng, "Jamming attacks and anti-jamming strategies in wireless networks: A comprehensive survey," *IEEE Commun. Surveys Tuts.*, vol. 9, no. 2, pp. 767–809, 2022.
- [14] G. Marti, O. Castañeda, S. Jacobsson, G. Durisi, T. Goldstein, and C. Studer, "Hybrid jammer mitigation for all-digital mmWave massive MU-MIMO," in *Proc. Asilomar Conf. Signals, Syst., Comput.*, Nov. 2021, pp. 93–99.
- [15] J. Zhu, Z. Wang, Q. Li, H. Chen, and N. Ansari, "Mitigating intended jamming in mmWave MIMO by hybrid beamforming," *IEEE Wireless Commun. Lett.*, vol. 8, no. 6, pp. 1617–1620, 2019.
- [16] X. Jiang, X. Liu, R. Chen, Y. Wang, F. Shu, and J. Wang, "Efficient receive beamformers for secure spatial modulation against a malicious full-duplex attacker with eavesdropping ability," *IEEE Trans. Veh. Technol.*, vol. 70, no. 2, pp. 1962–1966, 2021.
- [17] M. Chehimi, M. K. Awad, M. Al-Husseini, and A. Chehab, "Machine learning-based anti-jamming technique at the physical layer," *Concurrency and Computation: Practice and Experience*, vol. 35, no. 9, 2023.
- [18] G. Marti, O. Castañeda, and C. Studer, "Jammer mitigation via beamforming for low-resolution mmWave massive MU-MIMO," *IEEE Open J. Circuits Syst.*, vol. 2, pp. 820–832, 2021.
- [19] L. Yang, X. Jiang, F. Shu, W. Zhang, and J. Wang, "Estimation of covariance matrix of interference for secure spatial modulation against a malicious full-duplex attacker," *IEEE Trans. Veh. Technol.*, vol. 71, no. 8, pp. 9050–9054, Aug. 2022.
- [20] H. He, T. Su, H. Wang, Y. Teng, W. Shi, F. Shu, and J. Wang, "High-performance estimation of jamming covariance matrix for IRS-aided directional modulation network with a malicious attacker," *IEEE Trans. Veh. Technol.*, vol. 71, no. 9, pp. 10 137–10 142, Sep. 2022.
- [21] T. T. Do, E. Björnsson, E. G. Larsson, and S. M. Razavizadeh, "Jamming-resistant receivers for the massive MIMO uplink," *IEEE Trans. Inf. Forensics Security*, vol. 13, no. 1, pp. 210–223, Jan. 2018.
- [22] H. Akhlaghpasand, E. Björnsson, and S. M. Razavizadeh, "Jamming suppression in massive MIMO systems," *IEEE Trans. Circuits Syst. II*, vol. 68, no. 1, pp. 182–186, Jan. 2020.
- [23] H. Akhlaghpasand, E. Björnsson, and S. Razavizadeh, "Jamming-robust uplink transmission for spatially correlated massive MIMO systems," *IEEE Trans. Commun.*, vol. 68, no. 6, pp. 3495–3504, Jun. 2020.
- [24] H. Zeng, C. Cao, H. Li, and Q. Yan, "Enabling jamming-resistant communications in wireless MIMO networks," in *Proc. IEEE Conf. Commun. Netw. Security (CNS)*, Oct. 2017, pp. 1–9.
- [25] W. Shen, P. Ning, X. He, H. Dai, and Y. Liu, "MCR decoding: A MIMO approach for defending against wireless jamming attacks," in *Proc. IEEE Conf. Commun. Netw. Security (CNS)*, Oct. 2014, pp. 133–138.
- [26] Q. Yan, H. Zeng, T. Jiang, M. Li, W. Lou, and Y. T. Hou, "Jamming resilient communication using MIMO interference cancellation," *IEEE Trans. Inf. Forensics Security*, vol. 11, no. 7, pp. 1486–1499, Jul. 2016.
- [27] L. M. Hoang, J. A. Zhang, D. N. Nguyen, X. Huang, A. Kekirigoda, and K.-P. Hui, "Suppression of multiple spatially correlated jammers," *IEEE Trans. Veh. Technol.*, vol. 70, no. 10, pp. 10 489–10 500, 2021.
- [28] L. M. Hoang, D. Nguyen, J. A. Zhang, and D. T. Hoang, "Multiple correlated jammers suppression: A deep dueling Q-learning approach," in *Proc. IEEE Wireless Commun. Netw. Conf. (WCNC)*, Apr. 2022, pp. 998–1003.
- [29] G. Marti, T. Kölle, and C. Studer, "Mitigating smart jammers in multi-user MIMO," *IEEE Trans. Signal Process.*, vol. 71, pp. 756–771, 2023.
- [30] G. Marti and C. Studer, "Joint jammer mitigation and data detection for smart, distributed, and multi-antenna jammers," in *Proc. IEEE Int. Conf. Commun. (ICC)*, May 2023, pp. 1–6.
- [31] G. Marti and C. Studer, "Single-antenna jammers in MIMO-OFDM can resemble multi-antenna jammers," *IEEE Commun. Lett.*, vol. 27, no. 11, pp. 3103–3107, Nov. 2023.
- [32] E. S. Meckes, *The random matrix theory of the classical compact groups*. Cambridge University Press, 2019, vol. 218.
- [33] C. Eckart and G. Young, "The approximation of one matrix by another of lower rank," *Psychometrika*, vol. 1, no. 3, pp. 211–218, 1936.
- [34] A. P. Liavas and P. A. Regalia, "On the behavior of information theoretic criteria for model order selection," *IEEE Trans. Signal Process.*, vol. 49, no. 8, pp. 1689–1695, 2001.
- [35] K. B. Petersen and M. S. Pedersen, "The matrix cookbook," Nov. 2012.
- [36] G. Marti and C. Studer, "Joint jammer mitigation and data detection," in preparation.
- [37] J. Barzilai and J. M. Borwein, "Two-point step size gradient methods," *IMA J. Numer. Anal.*, vol. 8, no. 1, pp. 141–148, 1988.
- [38] T. Goldstein, C. Studer, and R. G. Baraniuk, "A field guide to forward-backward splitting with a FASTA implementation," Feb. 2016. [Online]. Available: <https://arxiv.org/abs/1411.3406>
- [39] R. P. Jover, J. Lackey, and A. Raghavan, "Enhancing the security of LTE networks against jamming attacks," *EURASIP J. Inf. Security*, vol. 2014, no. 1, pp. 1–14, 2014.
- [40] A. Omri, M. Shaqfeh, A. Ali, and H. Alnuweiri, "Synchronization procedure in 5G NR systems," *IEEE Access*, vol. 7, pp. 41 286–41 295, 2019.
- [41] G. Marti, F. Arqint, and C. Studer, "Jammer-resilient time-synchronization in the MIMO uplink," *arXiv preprint arXiv:2404.05335*.
- [42] N. Ailon and H. Rauhut, "Fast and rip-optimal transforms," *Discrete & Computational Geometry*, vol. 52, no. 4, pp. 780–798, 2014.
- [43] A. Andoni, P. Indyk, T. Laarhoven, I. Razenshteyn, and L. Schmidt, "Practical and optimal lsh for angular distance," *Advances in neural information processing systems*, vol. 28, 2015.
- [44] E. Borel, *Introduction géométrique à quelques théories physiques*. Gauthier-Villars, 1914.
- [45] B. D. Sutton, "The stochastic operator approach to random matrix theory," Ph.D. dissertation, Massachusetts Institute of Technology, 2005.
- [46] S. Jaeckel, L. Raschkowski, K. Börner, and L. Thiele, "QuaDRiGa: A 3-D multi-cell channel model with time evolution for enabling virtual field trials," *IEEE Trans. Antennas Propag.*, vol. 62, no. 6, pp. 3242–3256, Jun. 2014.
- [47] 3GPP, "3GPP TR 38.901," Mar. 2022, version 17.0.0.
- [48] 3GPP, "5G; NR; base station (BS) radio transmission and reception," Mar. 2021, TS 38.104 version 17.1.0 Rel. 17.
- [49] S. Dasgupta and A. Gupta, "An elementary proof of a theorem of johnson and lindenstrauss," *Random Structures & Algorithms*, vol. 22, no. 1, pp. 60–65, 2003.
- [50] Y. Chen, Y. Chi, J. Fan, C. Ma *et al.*, "Spectral methods for data science: A statistical perspective," *Foundations and Trends® in Machine Learning*, vol. 14, no. 5, pp. 566–806, 2021.